Palaeo-landslide dams controlled the formation of Late Quaternary terraces in Diexi, the upper Minjiang River, eastern Tibetan Plateau

Jingjuan Li[1], Xuanmei Fan[1], Zhiyong Ding[1], Shugang Kang[2], Marco Lovati[1]

[1] State Key Laboratory of Geohazard Prevention and Geoenvironment Protection, Chengdu University of Technology, Chengdu 610059, China

[2] State Key Laboratory of Loess and Quaternary Geology, Institute of Earth Environment, Chinese Academy of Sciences, Xi'an 710061, China

Correspondence to: Xuanmei Fan (fxm_cdut@qq.com)

Abstract

Tectonic uplift and climate changes are the two critical factors that control the evolution of river landscapes and the formation of terraces. However, the effect of river blockage events on terrace formation along valley areas remains poorly understood. In this paper, we investigated the geomorphology, sedimentology, and chronology of Tuanjie (seven staircases) and Taiping (three staircases) Terraces in Diexi. These represent two typical fluvial terraces in the upper Minjiang River in the eastern Tibetan Plateau. These terraces are composed, from bottom to top, of lacustrine deposits, gravels, loess, and paleosol. Field investigation, Digital Elevation Model (DEM) data, lithofacies, and dating results confirm that terraces T1 to T3 in Taiping correspond to terraces T5 to T7 in Tuanjie. Our findings suggest two damming and four outburst events occurred in the area since the late Pleistocene. The palaeo-dam blocked the river before 32 ka, followed by the first outburst at ~27 ka. Then, the palaeo-dam blocked the river again between 27 to 17 ka, and suffered a second dam-breaking event at ~17 ka. The third and fourth progressive collapse events respectively occurred at ~10 ka and ~9 ka. Our analysis, combined with the tectonic uplift rate, river incision rate, and high-resolution climate data, indicates that the blockage and collapse of the palaeo-dam have been a significant factor in the formation of tectonically active mountainous river terraces. Tectonic movement and climatic fluctuations, on the other end, play a minor role.

1 Introduction

Terraces, as a natural archive of the process of valley evolution, are used to explore the controlling mechanisms of river landscapes (Liu et al., 2021; Chen et al., 2020). This landform is sensitive to the impacts of tectonics and climate (Pan et al., 2003; Singh et al., 2017; Do Prado et al., 2022; Avsin et al., 2019; Gao et al., 2020). It can reflect the dynamics of the fluvial system (Schumm and Parker, 1973), rock uplift rate (Pan et al., 2013; Giano and Giannandrea, 2014; Malatesta et al., 2021), fault activity (Caputo et al., 2008), crustal movement (Westaway and Bridgland, 2007; Yoshikawa et al., 1964; Okuno et al., 2014), glacier melting (Oh et al., 2019; Vásquez et al., 2022; Bell, 2008), sea level (Malatesta et al., 2021; Yoshikawa et al., 1964) and lake level changes (Wang et al., 2021b). In tectonically active mountainous regions, some extreme events like landslides, debris flows, and rockfalls also change fluvial dynamics and landscapes (Molnar et al., 1993; Molnar and Houseman, 2013; Srivastava et al., 2017). Among these events, river blockages and sudden outbursts can strongly affect the evolutionary and geomorphology of the upstream and downstream sections (Hewitt et al., 2008; Hewitt et al., 2011; Korup et al., 2007; Korup et al., 2010). Currently, there are few studies on the influence of disaster events on the formation and evolution of terraces (Chen et al., 2016; Hu et al., 2018; Montgomery et al., 2004; Xu et al., 2020; Yuan and Zeng, 2012; Zhu et al., 2013), and further exploration is advisable.

The rapid uplift and climate change of the Tibetan Plateau in the late Quaternary led to frequent disaster events in its eastern margin (Yang et al., 2021; Dai et al., 2021; Wu et al., 2019; Gorum et al., 2011; Fan et al., 2018; Fan et al., 2017). As a result, the formation factors of river terraces in this region have been controversial, and the causes of the periodicity of the orbital scale (100 ka, 40 ka, 20 ka) and centennial-scale (0.1 ka) are also unclear.

The upper Minjiang River is located in the eastern Tibetan Plateau, and a wide distribution of three-tiered terraces characterizes it (Yang, 2005). The development of palaeo-landslides, climate variations, and the movement and evolution of regional tectonic uplift have been studied through these terraces. Due to the incompleteness of relevant data, these studies are still exploratory (Luo et al., 2019; Yang et al., 2003; Yang, 2005; Zhu, 2014; Gao and Li, 2006).

The terraces in the Diexi area are typical fluvial terraces in the upper Minjiang River, and they are located in the famous Diexi palaeo-dammed lake, which is one of the largest, best-preserved, and longest-duration lakes in a tectonically active mountainous region (Fan et al., 2019). Previous studies found two

terraces developed in Tuanjie and Taiping villages (Wang et al., 2005a; Yang et al., 2008; Fan et al., 2019). The analysis of lithofacies and sedimentary systems determined that the Diexi area is mainly composed of fluvial, lacustrine, alluvial fan and eolian sedimentary systems (Yang, 2005; Yang et al., 2008). Unfortunately, the systematic study of the Tuanjie and Taiping Terraces' sedimentary facies is incomplete. Currently, Tuanjie Terrace is thought to have resulted from the outburst of a palaeo-dammed lake 15000 years ago, and each terrace corresponds to different stages of outburst (Duan et al., 2002; Wang et al., 2005b; Wang, 2009; Zhu, 2014). This indicates that the Diexi palaeo-dammed lake has experienced at least one outburst flood event (Ma et al., 2018; Wang et al., 2012; Wang et al., 2005b). Moreover, the sedimentological analysis also suggests that the Diexi palaeo-dammed lake experienced at least two periods of blocking and outburst events (Yang, 2005; Yang et al., 2008), and four periods of fluvial progradation (Xu et al., 2020). Due to the lack of sedimentary sequence and chronological data, further study is needed on the evolution of palaeo-dam and the causes of terrace formation. The roles of tectonic activity, climate, river blockage and outburst events are crucial for discussing the formation of terrace staircases.

To explore the unsolved problems mentioned above, we investigated the geomorphological and sedimentological characteristics of the Tuanjie and Taiping Terraces using two independent dating methods, optically stimulated luminescence (OSL) and radiocarbon. The purposes of this paper are: (1) to clarify the deposition ages and sedimentary characteristics of Taiping and Tuanjie terraces; (2) to reveal the blockage and outburst of the palaeo-dam; (3) to explore the influences of tectonics, climate, and geological disasters (blocking and damming) on the formation of terraces.

2 Study area

The Diexi area is located in the upper reaches of the Minjiang River, which belongs to the northeast margin of the Tethys Himalayan domain and the Barkam formation zone, on the eastern margin of the Bayan Har Block (Fig. 1a). The Minjiang Valley is narrow at higher altitudes, and gradually widen downstream. The width varies from 60 to 300 m (Yang, 2005; Jiang et al., 2016; Ma, 2017; Zhang, 2019), and the steep slopes on both sides of the river valley have a gradient of 30-35° (Zhang et al., 2011; Guo, 2018), with a depth of 800 to 3000 m. Many outburst sediments are deposited downstream of Diexi, such

as Xiaoguanzi, Shuigouzi, and Manaoding (Fig. 1b).

Diexi palaeo-dammed lake (31º26′-33º16′ N; 102º59′-104º14′ E) is situated on the bend of the V-shaped Minjiang valley, which in turn lies in the well-known "north-south earthquake tectonic zone" (Tang et al., 1983; Huang et al., 2003; Yang, 2005; Deng et al., 2013). The palaeo-landslide that formed the Diexi palaeo-lake is located on the left bank of the Minjiang River, from the Jiaochang to the Diexi ancient town (Fig. 1b). The highest elevation of the palaeo-landslide is 3390 m, and the main slide direction is SW18°. The length and width of the palaeo-landslide are respectively about 3500 m and 3000 m, with a volume of the accumulation reaching 1.4 to 2.0×10^9 m^3 (Zhong et al., 2021). The elevation of the palaeo-landslide dam crest is 2500 m (Dai et al., 2023).

Diexi is located in the eastern Tibetan Plateau, and is being forged in the collision of the Indian and Eurasian plates (Fig. 1b). As the Tibetan Plateau and its surrounding areas have been affected by intense and frequent earthquakes during the late Quaternary (Yang et al., 1982; Chen and Lin, 1993; Li and Fang, 1998; Shi et al., 1999; Hou et al., 2001; Lu et al., 2004), Lake Diexi is influenced by active and accelerated tectonic activity. The area features visible strata from various periods: Devonian, Carboniferous, Permian, Triassic, and Quaternary (An et al., 2008; Zhang et al., 2011; Ma, 2017; Zhong, 2017). The Songpinggou River flows eastward as a tributary of the Minjiang River and merges into the Minjiang River in Lake Diexi. It has a typical alpine erosion landform with an 1868-4800 m elevation. Large amounts of Triassic sediments are deposited along the Songpinggou river bed.

The climate of the entire region is monsoonal, being influenced by the Plateau Monsoon, the Westerlies, and the East Asian Monsoon. The Diexi Valley, due to atmospheric circulation and the mountainous character, shows an arid and semi-arid climate (Shi, 2020). With the strong effect of the prevailing winds, the annual cumulative evaporation can reach 1000-1800 mm (Yang, 2005), and the average temperature and precipitation are 13.4℃ and 500-600 mm, respectively. Regarding ecological pattern, the vegetation shows a visible vertical zonation, composed mainly of mountain coniferous forests, alpine meadows, and low shrubs. The Songpinggou areas are scattered with forests of mountain pinus tabulaeformis, Sichuan-Yunnan alpine oak evergreen shrubs, and forests of deciduous species such as poplar and birch (Shi, 2020).

The seven staircases of Tuanjie Terrace (32º2′ N, 103º40′ E) are located in Tuanjie village, on the right bank of the Minjiang River, at the mouth of the Songpinggou tributary (Fig. 1c). The three staircases of Taiping Terrace (32º12′13″ N, 103º45′53″ E) are in Taiping village, at the mouth of Luobogou Gully,

which is 12 km upstream of the Tuanjie Terrace (Fig. 1d) (Fan et al., 2021; Wang et al., 2005b). The course of the river from Taiping to Manaoding is a deep canyon (Duan, 2002), despite the Taiping and Tuanjie area being a broad valley landform.

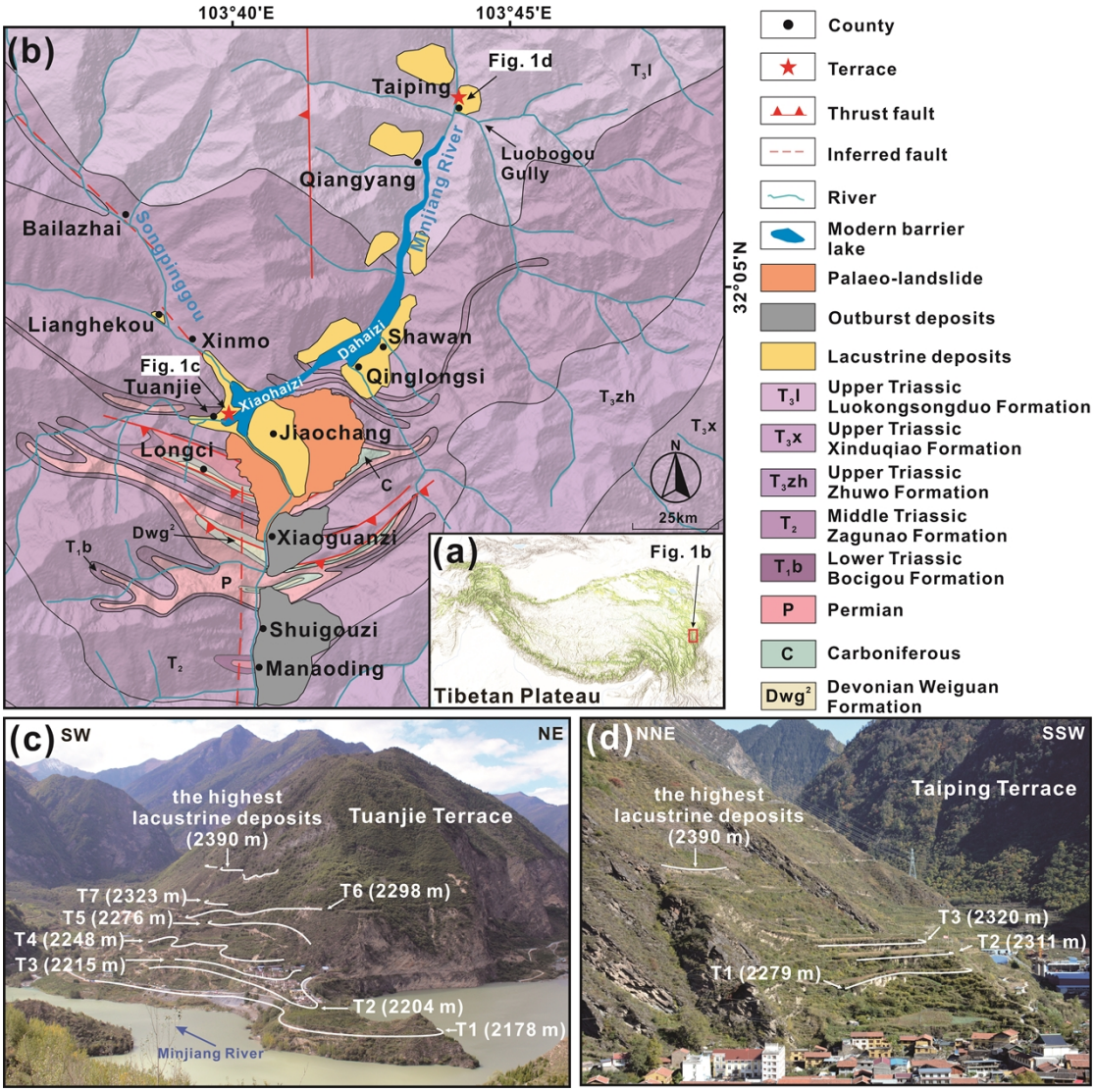

Figure 1. Location of the study area. (a) Overview of the Diexi area at the eastern margin of the Tibetan Plateau. (b) Geological characteristics of Diexi area and legends (maps modified from Guo, 2018; Wang et al., 2020a; Zhong et al., 2021). (c) The topography of the Tuanjie Terrace. (d) The topography of the Taiping Terrace. The elevation of each terrace level is shown in (c) and (d).

3 Materials and methods

3.1 Geomorphic and sedimentary description

From October to November 2018, field surveys were carried out in the Diexi area. These terraces

are named in order of Terrace 1 (T1) to Terrace 7 (T7) from bottom to top. The sedimentary structure, geometric shape, sorting, roundness, and the direction of gravels are described. The lithofacies of the Diexi palaeo-dammed lake were analyzed using the classification method of sedimentary facies (Miall, 2000) and previous research conducted in the Diexi area (Yang, 2005; Yang et al., 2008) (Table. 1).

Table. 1 Lithofacies of Diexi area, eastern Tibet Plateau. Adapted from Miall (2000), Yang (2005) and Yang et al. (2008).

Lithofacies code	Lithofacies	Sedimentary structures	Interpretation
Ps	Paleosol	Pedogenic features, roots	Pedogenesis
Ls	Sandy loess	Massive texture	Eolian deposits
Gmm	Matrix-supported, massive gravel	Weak grading	Plastic debris flow (high-strength, viscous)
Gh	Clast-supported, crudely bedded gravel	Horizontal bedding, imbrication	Longitudinal bedforms, lag deposits, sieve deposits
Gci	Clast-supported gravel	Inverse grading	Clast-rich debris flow (high strength), or pseudoplastic debris flow (low strength)
Gcm	Clast-supported, massive gravel	-	Pseudoplastic debris flow (inertial bedload, turbulent flow)
Fm	Mud	snail shells	Overbank, abandoned channel, or drape deposits
Fl	silty clay	parallel bedding, wave bedding	Lacustrine deposits

3.2 Chronology

Two independent dating methods were employed to establish a reliable chronostratigraphic framework: OSL and radiocarbon. To clarify the damming and outburst processes of the palaeo-dam, and the stability time of terraces, we collected samples from the top of lacustrine and gravel units, and the bottom of loess and paleosol units. A total of twenty-two samples were obtained from the Tuanjie and Taiping terraces. Of these, nineteen have been dedicated to OSL dating, while the other three have been allocated to radiocarbon dating (Fig. 2).

3.2.1 OSL dating

Nineteen OSL samples were collected from lacustrine deposits, gravel units, loess, and paleosol

(Fig. 2 and 3). In Tuanjie Terrace, twelve samples were collected from the lacustrine deposits, excluding T6 and the highest lacustrine deposits. Two samples were collected from the gravel units of T2 and T5, and the paleosol samples were taken from T1 to T5 and T7 terraces (Fig. 2 and 3). In Taiping Terrace, four samples were taken from the lacustrine deposits at the T1 to T3 terraces and the highest deposits, and another one was taken from the paleosol unit at the T3 terrace (Fig. 2 and 3). To ensure that human activities and modern weathering did not disturb the samples, we scraped the surface sediments, and pushed the stainless steel tubes with a hammer to collect shielded deposits. After the tubes were took out from the fresh sections, both ends of the tube were sealed with black opaque tape.

Samples were processed and measured at the Institute of Earth Environment, Chinese Academy of Sciences. The quartz grains were extracted following the laboratory pre-treatment procedures (Kang et al., 2020; Kang et al., 2013). The sediments at the two ends of the tubes, which may be exposed to daylight during sampling, were removed. And, the unexposed samples were prepared for equivalent dose (D_e) and environment dose rate determination. Approximately 50 g samples were treated with 30% HCl and 30% H_2O_2 to remove carbonates and organic matter, respectively. Then, the samples were washed with distilled water until the pH value of the solution reached 7. For samples IEE5542 and IEE5550, the coarse fractions (90-150 μm) were sieved out and etched with 40% HF for 45 mins, followed by washing using 10% HCl and distilled water. For the other 17 samples, the fine polymineral grains（4-11 μm）were separated according to the Stokes' law. These fine polymineral grains were immersed in 30% H_2SiF_6 for 3-5 days in an ultrasonic bath to extract quartz. Finally, the purified fine (coarse) quartz was deposited (mouted) on stainless steel discs with a diameter of 9.7 mm for experimental use. The purity of quartz was verified by IRSL intensity and OSL IR depletion ratio (Figs. S1 and S2a; Duller, 2003).

All OSL measurements were performed on a Lesxyg Research measurement system, with blue light at (458±10) nm, and infrared light at (850±3) nm for stimulation and a $^{90}S/^{90}Y$ beta source (~0.05 Gy/s) for irradiation. Luminescence signals were detected by an ET 9235QB photomultiplier tube (PMT) through a combination of U340 and HC340/26 glass filters.

The single-aliquot regenerative-dose (SAR) protocol (Table. S1; Murray and Wintle, 2000; Wintle and Murray, 2006) was utilized to determine the Equivalent Dose (D_e), as used in Kang et al. (2020). Quartz grains were preheated at 260°C for 10 s for natural and regenerative-dose, and a cut-heat at 220°C for 10 s was applied for test dose. The quartz was stimulated for 60 s at 125°C with blue LEDs. The OSL signal was calculated as the integrated value of the first 0.5 s of the decay curve minus the integrated

value of the last 0.5 s as the background. For D_e determination, approximately 10 aliquots were measured for each sample. And, the mean D_e value of all aliquots was used as the final D_e value. Conventional tests in SAR protocol, including recuperation ratio, recycling ratio, quartz OSL brightness and fast-component dominated nature, growth curve shape, and D_e distribution (Figs. S2 and S3), indicate that the protocol can be robustly used to date the samples in this study.

The environmental dose rate was estimated from the radioisotope concentrations (uranium, thorium, and potassium) and cosmic dose rates. U and Th concentrations were determined by inductively coupled plasma mass spectrometry (ICP-MS), while K concentration was measured by inductively coupled plasma optical emission spectrometry (ICP-OES). The cosmic dose rates were calculated using the equation proposed by Prescott and Hutton (1994). The α-value of fine (4-11 μm) grained quartz was assumed to be 0.04±0.002 (Rees-Jones, 1995). Considering the current climate conditions, the sedimentary facies, and past climate changes since the sample deposition, the water content of the gravel and paleosol was assumed to be 10±5%, while the water content of lacustrine deposits was estimated to be 20±5%. Dose rate was calculated using the Dose Rate and Age Calculator (DRAC) (Durcan et al., 2015). Finally, the quartz OSL ages were obtained by dividing the measured D_e (Gy) by the environmental dose rate (Gy/ka).

3.2.2 Radiocarbon

Three samples were obtained for radiocarbon analysis, including two samples from the highest lacustrine deposits in the Tuanjie and Taiping Terraces, and one sample from the overlying loess of the T4 terrace in Tuanjie (Fig. 2 and 3). The AMS ^{14}C sample collected from the top of the Taiping Terrace was used for comparison with the OSL sample (TP19-1), which was taken from the same position. The AMS ^{14}C sample collected from the top of the Tuanjie Terrace was compared with the AMS ^{14}C dating of the top of the Taiping Terrace. Utilizing the same dating method for age comparison enhances credibility. Field investigations showed that the loess unit of the Tuanjie T4 was the most complete and easier to collect, therefore, we collected the loess sample from T4. The surface sediments were removed to avoid the influence of weathering.

All the samples were tested for organic matter, and analyzed using the NEC accelerator mass spectrometer and Thermo infra-red mass spectrometer at the Beta Analytic Radiocarbon Dating

Laboratory. The samples were pre-treated following their protocols. The ages were then converted into calendar years using the IntCal 20 calibration curve (Reimer et al., 2020).

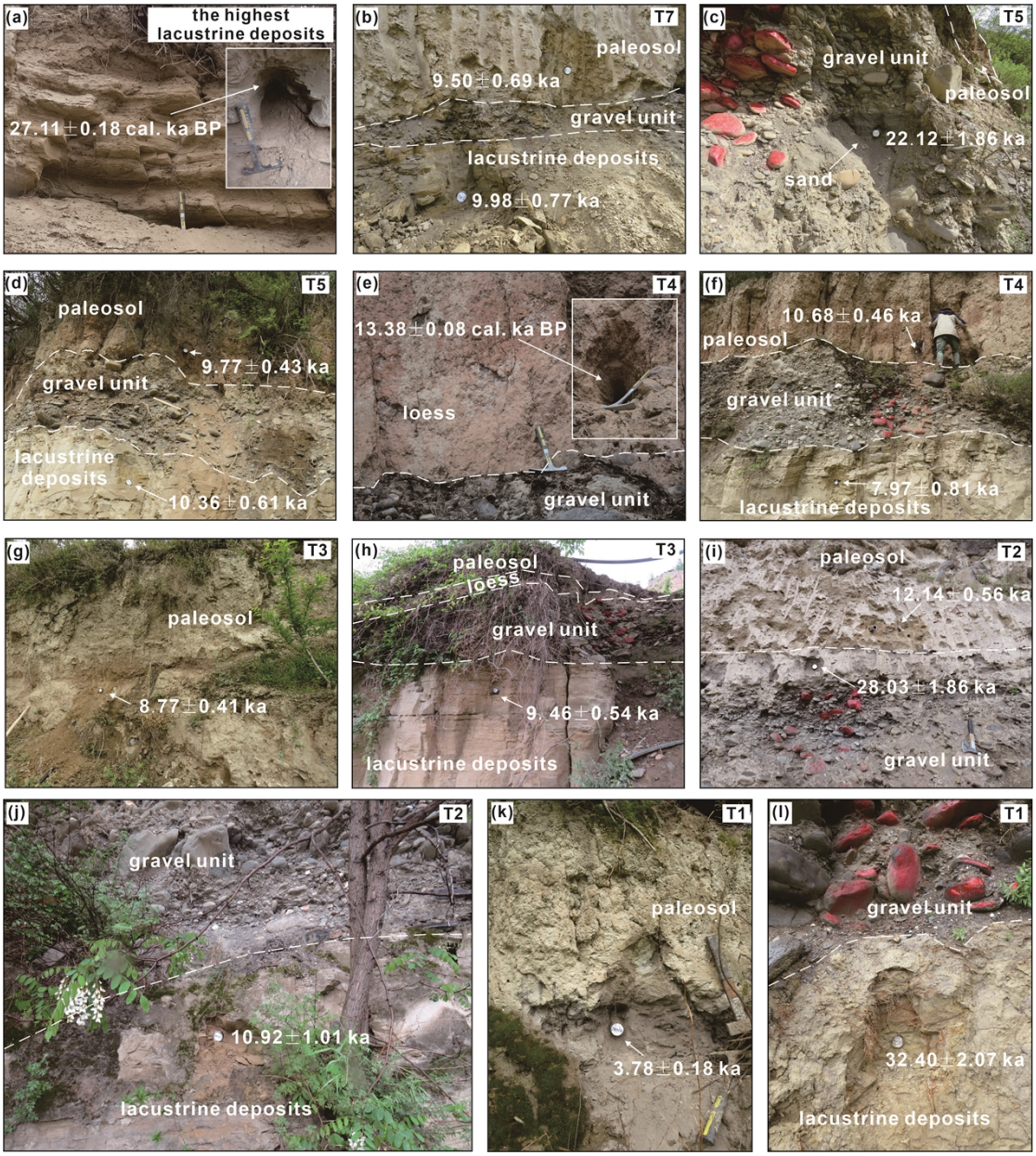

Figure 2. OSL and radiocarbon samples from Tuanjie Terrace. (a) Radiocarbon sample of the highest lacustrine deposits. (b) OSL samples of the lacustrine deposits and paleosol in T7. (c) OSL sample from the gravel unit in T5. (d) OSL samples of the lacustrine deposits and paleosol in T5. (e) Radiocarbon sample of loess in T4. (f) OSL samples of the lacustrine deposits and paleosol in T4. (g) OSL sample of the paleosol in T3. (h) OSL sample of the lacustrine deposits in T3. (i) OSL samples of the gravel unit and paleosol in T2. (j) OSL sample of the lacustrine deposits in T2. (k) OSL sample of the paleosol in T1. (l) OSL sample of the lacustrine deposits in T1. The white dashed line marks the boundary between units (same as shown below).

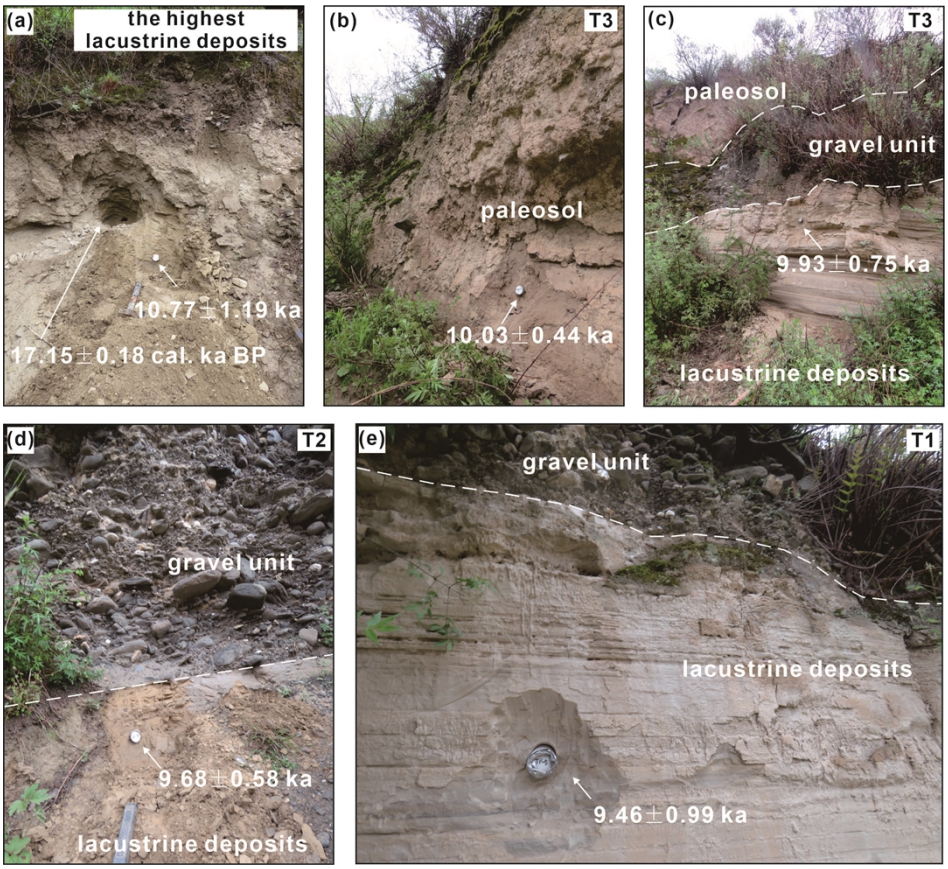

Figure 3. OSL and radiocarbon samples were taken from Taiping Terrace. (a) Paired OSL and radiocarbon samples were collected from the highest lacustrine deposits. (b) OSL sample of paleosol in T3. (c) OSL sample of the lacustrine deposits in T3. (d) OSL sample of the lacustrine deposits in T2; (e) OSL sample of the lacustrine deposits in T1.

4 Results

4.1 Terraces distribution

Tunajie Terrace has seven staircases, Taiping Terrace has three staircases, all of which are based on lacustrine deposits (Fig. 4). The thickness of lacustrine deposits in Tuanjie Terrace is >200 m, and the lateral lengths of the seven terraces range from 150 to 1000 m (Fig. 4), Terrace T1 has the most significant extension towards the center of the Diexi Lake (Fig. 1c). Taiping terraces developed on the hillside with a slope of 40°-60°, influenced by landslides and croplands. The horizontal extensions of T1, T2, and T3 are equal to 520 m, 380 m, and 190 m, respectively.

Terrace elevations were obtained using the Light Detection And Ranging (LiDAR) with a 0.5 m accuracy and the Advanced Spaceborne Thermal Emission and Reflection Radiometer Global Digital Elevation Model (ASTER GDEM) with a 30 m accuracy (Fan et al., 2021). The data were imported in

ArcGIS 10.3, and field investigations on two Terraces determined their altimetric level (Table. 2), textures, and formation ages (Fig. 4). The elevation data reported in Fig. 1c and 1d show the elevations of all the terrace surfaces.

Table. 2 Elevation of the Tuanjie and Taiping terraces.

Tuanjie Terrace	Elevation (m)	Taiping Terrace	Elevation (m)
Highest	2390	Highest	2390
T7	2323	T3	2320
T6	2298	T2	2311
T5	2276	T1	2279
T4	2248	-	-
T3	2215	-	-
T2	2204	-	-
T1	2178	-	-

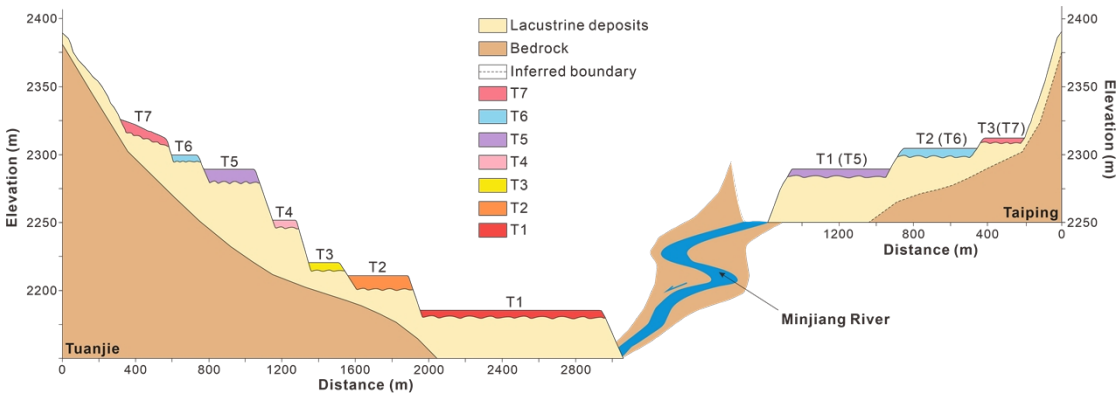

Figure 4. Correlation between the Tuanjie and Taiping terraces. Elevation data showed that Taiping T1 to T3 corresponded to Tuanjie T5 to T7, respectively.

4.2 Terraces lithostratigraphy

We have summarized the lithology, texture, and sedimentary structures of the Tuanjie and Taiping terraces.

4.2.1 Tuanjie Terrace

The lithostratigraphy of the Tuanjie terraces, from bottom to top, is summarized as follows (Table. 1 and Fig. 5a): (1) Silt clay (*Fl*), this unit has intense weathering, horizontal bedding, and wave bedding,

indicating the presence of lacustrine deposits. (2) Gravel units (*Gh, Gci, Gmm*) represent fluvial deposits and display an unconformity with the underlying layers. The orientation of the gravels is predominantly parallel to the Minjiang River, suggesting that the Minjiang River is the source of these gravels. The gravel units in Tuanjie T1, T4, T5, and T7 (*Gh*) are generally poorly sorted and well-rounded, with a diameter ranging from 2 to 30 cm. This indicates the presence of longitudinal bedforms, lag deposits, and sieve deposits (Fig. 5a). Gravels in Tuanjie T2 (*Gci*) have a 2-25 cm diameter and exhibit inverse grading. Gravels larger than 35 cm in diameter are rare, and the gravels are poorly sorted and sub-circular to round, lacking a specific direction. In Tuanjie T3 (*Gci*), the gravel units are poorly sorted and sub-circular to round gravels with a 3-25 cm diameter and exhibit inverse grading. These features suggest that the gravel units of T2 and T3 are clast-rich debris flows with high strength or pseudoplastic debris flows with low strength. Gravels in Tuanjie T6 (*Gmm*) have graded bedding with well sorting and rounding, indicating deposition by plastic debris flows with high strength. (3) Loess (*Ls*), loess units of T1 and T2 are brick-red in color. Angular phyllites occur in T3. (4) Paleosol (*Ps*), this unit caps all terraces, and is characterized by abundant roots (Fig. 5a). Above T7, lacustrine deposits with a thickness of 30 m are present, exhibiting undulating bedding and severe denudation. The highest point of lacustrine deposits reaches up to 2390 m (Fig. 5a).

The strata of each terrace exhibit variations. Terraces T1, T2, T3, T4, and T6 are characterized by a sequence of lacustrine, gravels, loess, and paleosol units, whereas T5 and T7 lack the loess unit (Fig. 5a). The absence of loess units in T5 and T7 may be caused by erosion and human activities. It is noteworthy that terraces T4 to T7 have undergone varying degrees of deformation and collapse. The deformation can be attributed to cultivation, excavation, and human activity. Additionally, natural disasters may have also contributed to the deformation. Further research is necessary to establish the precise causes of the deformation observed in these terraces.

4.2.2 Taiping Terrace

In Taiping, a set of three terraces also has a base consisting of lacustrine deposits, as Fan et al. (2021) documented. The sedimentary sequences of Terraces T1 and T2 are comparable to T5 and T6 of the Tuanjie Terrace (Fig. 5). Taiping T1 is covered by gravels and paleosol, while T2 is characterized by a sequence of gravels, loess and paleosol (Fig. 5b). Terrace T3, however, has distinct features. It consists

of a gravel unit (*Gcm*) overlying two sequences of mud (*Fm*)-phyllite clasts (*Gh, Gci*) layers (Fig. 5b). The mud layers in T3 contain snail shells, and the two clast layers are composed of neatly arranged phyllites (Fig. 5b).

The three gravel units observed in the Taiping terraces have a directional pattern along the Luobogou Gully, indicating their origin from a high-energy event within the gully. Gravels in Taiping T1 (*Gcm*) are characterized by poorly sorted and subrounded gravels with a diameter of 5-10 cm, implying the presence of a pseudoplastic debris flow (Fig. 5). Similarly, the gravel units in Taiping T2 and T3 (*Gcm*) contain numerous broken phyllites, indicating the occurrence of pseudoplastic debris flows. The loess units in Taiping T2 and T3 (*Ls*) are mixed with 2-5 cm diameter of angular phyllites. This feature suggests the presence of high-energy environments that facilitated the mixing of loess with phyllite clasts. Furthermore, the two mud-phyllite clasts layers in Taiping T3, indicate the occurrence of two blocking events. The presence of snail shells within the mud layers suggests the occurrence of overbank deposits, abandoned channels, or drape deposits (Fig. 5).

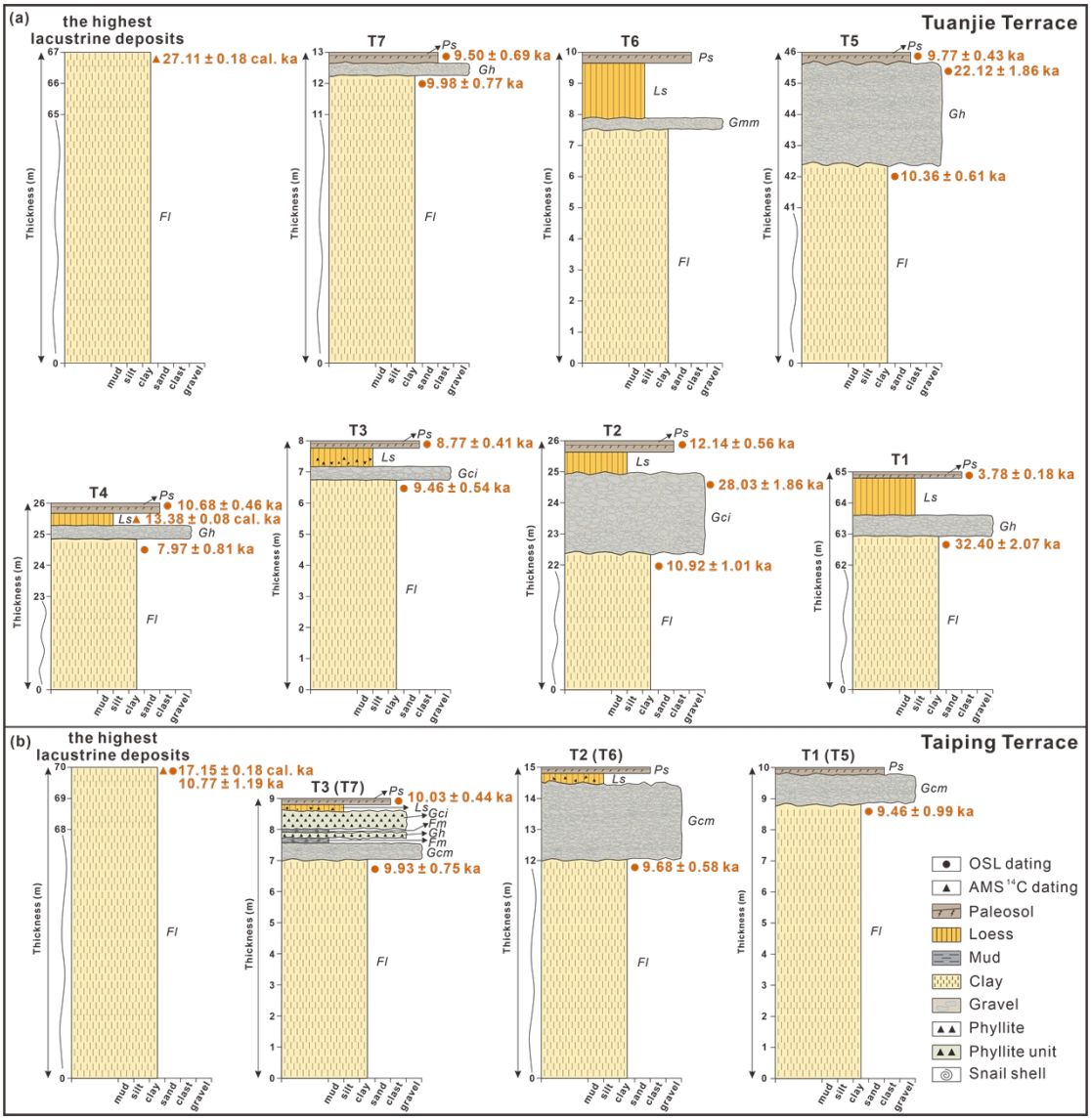

Figure 5. Sedimentary deposits, lithofacies, and chronologies of the Tuanjie and Taiping terraces. (a) T1, T2, T3, T4, T5, T6, T7, and the highest lacustrine deposits of the Tuanjie terraces, respectively. Terraces T1 to T4 and T6 are composed, from bottom to top, of lacustrine deposits, gravels, loess, and paleosol. The loess of T3 contains phyllites. The sedimentary sequence of T5 and T7 comprises lacustrine deposits, gravels, and paleosol. (b) T1, T2, T3, and the highest lacustrine deposits of the Taiping terraces. Terrace T1 is composed of lacustrine deposits, gravels, and paleosol, from bottom to top. The sequence of T2 is lacustrine deposits, gravels, loess, and paleosol. In T3, there are two sets of mud-phyllite clasts layers deposited between the gravel unit and loess. The loess in T2 and T3 is mixed with phyllites. Terraces T1 to T3 in Taiping correspond to terraces T5 to T7 in Tuanjie. OSL and radiocarbon dating results are denoted. Lithofacies are coded in Table. 1.

4.3 OSL ages

We obtained 19 quartz OSL ages, with 14 ones from the Tuanjie terraces and the other 5 ones from the Taiping terraces, as presented in Table 3.

OSL dating of lacustrine deposits in Tuanjie terraces yielded ages of 32.40±2.07 ka for the T1, 10.92±1.01 ka for the T2, 9.46±0.54 ka for the T3, 7.97±0.81 ka for the T4, 10.36±0.61 ka for the T5 and 9.98±0.77 ka for the T7. Consequently, T1 was deposited in the late Pleistocene; T2, T5, and T7 were deposited at the beginning of the Holocene; T3 was deposited at the end of the early Holocene; and T4 was deposited at the beginning of the middle Holocene. The chronological results of lacustrine deposits are chaotic. Tuanjie T1-T4 becomes younger with increasing elevation. Tuanjie T5 and T7 have a similar age, but are older than T3 and T4. The highest lacustrine deposits are only about 5 ka younger than T1. Dating results of gravels from the T2 and T5 show that these were deposited in the late Pleistocene, and the ages are 28.03±1.86 ka and 22.12±1.86 ka, respectively. The ages of the paleosol of each terrace differ, but most paleosol units were deposited during the Holocene. Paleosol of T2 and T4 were deposited at the older ages of 12.14±0.56 ka and 10.68±0.46 ka, respectively. And the paleosol units of T3, T5, and T7 are deposited at 8.77±0.41 ka, 9.77±0.43 ka, and 9.50±0.69 ka, respectively. T1 has the youngest paleosol unit with an age of 3.78±0.18 ka.

The OSL ages of Taiping T1 to T3 lacustrine deposits are 9.46±0.99 ka, 9.68±0.58 ka, and 9.93±0.75 ka, respectively. The highest lacustrine deposits yielded an age of 10.77±1.19 ka. All the terraces were deposited during the Holocene.

Table. 3 OSL ages, radioisotope, water content, and dose rate of OSL samples at the Tuanjie and Taiping Terraces.

Location	Deposit level	Facies	Longitude and latitude	Lab code	Quartz grain size (μm)	Sample ID	Elevation (m)	Depth (m)	U (ppm)	Th (ppm)	K (%)	Water content (%)	Dose rate (Gy/ka)	Dose (Gy)	Age (ka)
Taiping	-	lacustrine	32°7′37″N, 103°44′14″E	IEE5554	4-11	TP19-1	2342.95	1.90	4.82±0.14	12.85±0.37	1.98±0.03	20±5	4.27±0.14	45.93±4.84	10.77±1.19
	T3	paleosol	32°7′34″N, 103°44′12″E	IEE5555	4-11	TP19-2	2279.14	3.50	2.92±0.05	14.75±0.20	2.01±0.02	10±5	4.28±0.15	42.95±1.10	10.03±0.44
		lacustrine		IEE5556	4-11	TP19-3		4.20	3.62±0.55	14.23±0.27	2.20±0.04	20±5	4.17±0.16	41.43±2.68	9.93±0.75
	T2	lacustrine	32°7′32″N, 103°44′11″E	IEE5557	4-11	TP19-4	2219.57	3.60	3.29±0.10	12.59±0.40	1.90±0.01	20±5	3.71±0.12	35.89±1.80	9.68±0.58
	T1	lacustrine	32°7′33″N, 103°44′11″E	IEE5558	4-11	TP19-5	2177.27	1.00	3.31±0.07	12.74±0.19	2.17±0.02	20±5	4.02±0.13	38.05±3.78	9.46±0.99
Tuanjie	T7	paleosol	32°2′42″N, 103°39′45″E	IEE5540	4-11	DX19-1	2315.45	2.30	3.48±0.04	13.86±0.28	2.16±0.07	10±5	4.54±0.17	43.16±2.71	9.50±0.69
		lacustrine		IEE5541	4-11	DX19-2		2.90	3.41±0.05	14.00±0.20	2.40±0.05	20±5	4.29±0.14	42.82±2.99	9.98±0.77
	T5	paleosol	32°2′42N, 103°39′48″E	IEE5543	4-11	DX19-4	2265.88	1.30	2.93±0.07	13.49±0.21	2.03±0.02	10±5	4.25±0.15	41.47±1.05	9.77±0.43
		fluvial	32°2′46″N, 103°39′55″E	IEE5542	90-150	DX19-3	2264.93	2.60	2.28±0.05	10.25±0.17	1.53±0.04	10±5	2.70±0.11	59.74±4.46	22.12±1.86
		lacustrine	32°2′42″N, 103°39′48″E	IEE5544	4-11	DX19-5	2265.88	2.80	3.14±0.05	13.34±0.13	2.16±0.05	20±5	3.96±0.13	41.03±1.98	10.36±0.61
	T4	paleosol	32°2′40″N, 103°39′56″E	IEE5545	4-11	DX19-6	2228.79	2.20	2.85±0.03	14.35±0.10	2.00±0.01	10±5	4.24±0.15	45.33±1.14	10.68±0.46
		lacustrine		IEE5546	4-11	DX19-7		5.00	3.57±0.06	14.13±0.36	2.45±0.04	20±5	4.34±0.15	34.59±3.33	7.97±0.81
	T3	paleosol	32°2′40″N, 103°39′55″E	IEE5547	4-11	DX19-8	2192.44	2.20	2.99±0.29	12.78±0.19	1.96±0.07	10±5	4.11±0.16	36.05±0.91	8.77±0.41
		lacustrine		IEE5548	4-11	DX19-9		2.10	3.12±0.16	13.54±0.21	2.48±0.02	20±5	4.26±0.14	40.26±1.85	9.46±0.54
	T2	paleosol	32°2′46″N, 103°39′60″E	IEE5549	4-11	DX19-10	2180.47	5.00	3.40±0.05	13.97±0.23	2.41±0.06	10±5	4.70±0.18	57.06±1.52	12.14±0.56
		fluvial		IEE5550	90-150	DX19-11		5.50	3.37±0.04	14.74±0.12	1.78±0.04	10±5	3.38±0.13	94.60±5.09	28.03±1.86
		lacustrine	32°2′42″N, 103°40′08″E	IEE5551	4-11	DX19-12	2193.80	4.50	3.35±0.04	13.76±0.16	2.26±0.07	20±5	4.10±0.14	44.79±3.84	10.92±1.01
	T1	paleosol	32°2′41″N, 103°40′11″E	IEE5553	4-11	DX19-14	2148.88	0.60	2.38±0.07	8.69±0.29	1.52±0.07	10±5	3.20±0.13	12.09±0.30	3.78±0.18
		lacustrine	32°2′43″N, 103°40′13″E	IEE5552	4-11	DX19-13	2150.60	2.50	2.89±0.03	11.81±0.10	2.16±0.05	20±5	3.77±0.13	122.24±6.67	32.40±2.07

* Terraces are not completely flat, so the elevation data of some samples deviate from the elevation of the terrace.

4.4 AMS ^{14}C ages

The highest lacustrine deposits of the Tuanjie and Taiping Terraces were deposited at 27.11±0.18 cal. ka BP and 17.15±0.18 cal. ka BP, respectively. Additionally, the loess in T4 of the Tuanjie Terrace was deposited at 13.38±0.08 cal. ka BP (Table 4).

Table. 4 Radiocarbon results for the Tuanjie and Taiping Terraces.

Samples	Lab code	Material	Elevation (m)	$\delta^{13}C$ (‰)	Radiocarbon age (a BP)	Calibration age (cal. ka BP)
TP-max	Beta-520926	bulk sediment	2342.95	-19.1	14050±50	17.15±0.18
TJ-max	Beta-520925	bulk sediment	2390.00	-19.2	22740±90	27.11±0.18
TJ-T4-HT	Beta-520924	bulk sediment	2280.00	-21.6	11490±40	13.38±0.08

5 Discussion

5.1 Reliability of dating results

Considering the fine silt dominated nature, the relatively stable depositional environment, and the normal distribution of D_e particularly for the two coarse samples, we assume that all the OSL samples were well bleached before deposition. Although the lacustrine deposits from Tuanjie T1 yielded an age of 32.40±2.07 ka (DX19-13, Fig. 5a), the reliability of this sample is supported by the basal age of the ZK2 core (35.13±0.29 cal. ka BP, Wang et al., 2012) and the upper and lower age limits of the Tuanjie section (35.78±0.37~30.66±0.03 cal. ka BP, Zhang et al., 2009). Comparing all the ages within the Tuanjie Terraces, the gravel units have older ages (Fig. 5). However, these two fluvial deposits have the similarity ages with the convolution structures in Haizipo (27.24±0.41 cal. ka BP, 27.74±0.47 cal. ka BP; Wang et al., 2012), suggests the reliability of the gravel ages. The gravel units in Tuanjie T2 and T5 and the convolution structures in Haizipo were formed concurrently.

The highest lacustrine deposits in Taiping underwent paired radiocarbon and OSL dating, resulting in ages of 17.15±0.18 cal. ka BP and 10.77±1.19 ka, respectively (Fig. 5). The discrepancy between the two dating methods reveals that the radiocarbon age appears to be approximately 6,000 years than the OSL age. This difference suggests a potential overestimation of radiocarbon ages due to the old carbon

effect. Several factors contribute to the reservoir effect, including: (1) lower ^{14}C specific activity in water compared to the atmosphere (Deevey et al., 1954). (2) subaqueous landslides, slumps, or other disturbances may have mixed older sediments with younger ones (Counts et al., 2015; Shi, 2020). (3) the re-deposition of older organic components, leading to a pre-dating bias in the biological indicators of sediments (Kaplan et al., 2017; Krivonogov et al., 2016).

Besides, previous studies show the terrace ages of the lacustrine deposits along the Diexi area are mainly between 35.78 and 10.63 ka (Table. S2). Our dating results of lacustrine deposits lie within this range, supporting our data are reliable.

5.2 Terraces along the upper Minjiang River

Along the upper Minjiang River, there are a minimum of twenty-two terraces, with eleven terraces located upstream of the Diexi area (from Zhangla to Gonggaling), four sites near the Diexi area (Taiping, Shawan, Jiaochang, and Tuanjie areas), and seven sites are developed downstream (from Maoxian-Wenchuan). A total of 124 samples for terrace dating were collected from these sites (Table. S2), including thirty-two samples from the upstream, eighty-three samples from the Diexi area, and nine samples from the downstream. The ages of the upstream terraces indicate that the formation and evolution of terraces in the upper Minjiang River began around 830 ka (the early Pleistocene, Zhao et al., 1994), and primarily formed between 47-2 ka (Fig. 6). The terraces in the Diexi area have ages that are distributed between 550 and 50 ka (Duan et al., 2002; Guo, 2018; Kirby et al., 2000; Wang et al., 2020b; Wang et al., 2007; Wang, 2009; Yang et al., 2003; Zhong, 2017; Gao and Li, 2006; Jiang et al., 2014; Luo et al., 2019; Mao, 2011; Zhang, 2019), with the majority observed between 32-2 ka (Fig. 6). Downstream terraces were deposited between 400 and 50 ka (Yang et al., 2003; Yang, 2005; Zhao et al., 1994; Zhu, 2014), with a significant portion formed between 40 to 20 ka (Fig. 6). In summary, the terrace ages along the upper Minjiang River span from 830 to 1 ka, with the majority formed between 40 and 6 ka. The Diexi area shows a higher concentration of terraces than the upstream and downstream regions, with these terraces primarily formed from 30 to 0 ka.

The terraces in the area stretching from the Zhangla basin to the source of the Minjiang River are attributed to tectonic uplift (Yang et al., 2003; Yang, 2005; Yang et al., 2011; Yang et al., 2008; Chen and Li, 2014; Zhu, 2014). In the Diexi area, the formation and evolution of the Tuanjie and Taiping

Terraces were influenced by the evolution of a palaeo-dam (Duan et al., 2002; Wang et al., 2005b; Wang, 2009; Zhu, 2014). The terraces in the Maoxian-Wenchuan region share similar features with the terraces in Diexi, as they are also believed to have formed as a result of the outburst of a palaeo-dammed lake (Zhu, 2014). These results indicate that the terrace formation mechanism downstream differs from that upstream. However, sufficient evidence has not been presented to support this perspective. In the following sections, we will present additional evidence to explore this phenomenon further.

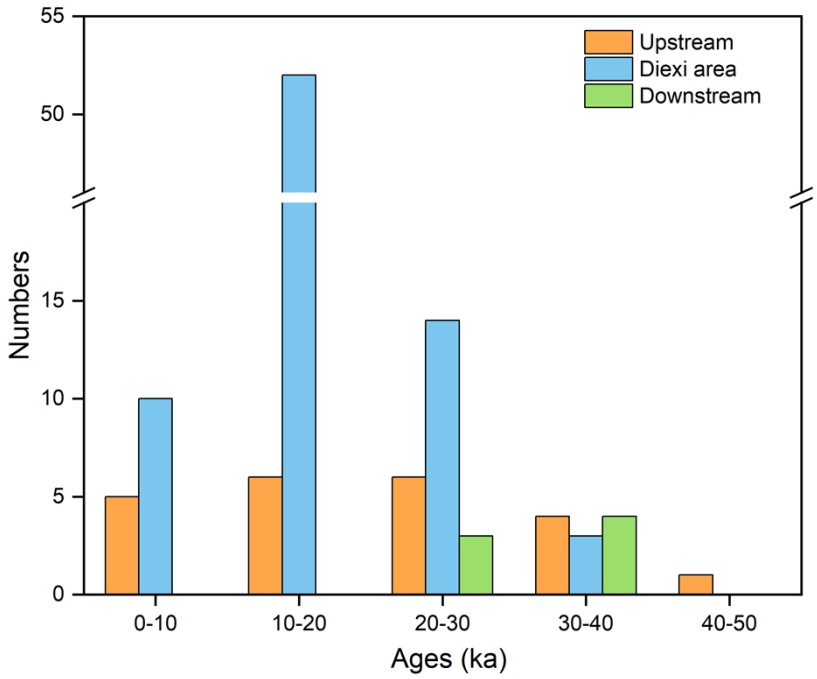

Figure 6. Frequency distribution histogram of terrace ages since 50 ka in the upper reaches of the Minjiang River. The terraces ages of the upstream area are distributed between 46.40 ka to 2.81 ka. The terraces ages of the Diexi area range from 35.78 and 3.70 ka. The ages of the terraces downstream are distributed in 39.90 to 20.70 ka. Terraces developed in the Diexi area were mainly formed during 30-8 ka.

5.3 Correlation of the Tuanjie and Taiping Terraces

The highest lacustrine deposits in Tuanjie and Taiping have equal elevation (2390 m), suggesting that Taiping Terrace and Tuanjie Terrace are somehow related.

Other evidence comes from the characteristics of sedimentary stratigraphy, thus the T1 to T3 terraces of Taiping correspond to the T5 to T7 terraces of Tuanjie (Fig. 4). Terrace T5 (Tuanjie) and T1 (Taiping) have the same sedimentary sequences from the bottom to the top, including clays (*Fl*), gravel unit (*Gh* in Tuanjie, *Gcm* in Taiping) and paleosol (*Ps*) (Fig. 5a and 5b). Paleosol (*Ps*) in T5 (Tuanjie)

and T1 (Taiping) are 0.4 m and 0.2 m thick, respectively. Both T6 (Tuanjie) and T2 (Taiping) have the sequences of clays (*Fl*), gravel unit (*Gmm* in Tuanjie, *Gcm* in Taiping), loess (*Ls*), and paleosol (*Ps*). The sedimentary successions of Terrace T7 (Tuanjie) and T3 (Taiping) are both clays (*Fl*), gravel unit (*Gh* in Tuanjie, while *Gcm* in Taiping), and paleosol (*Ps*). T3 of Taiping has two sets of mud-phyllite clasts (*Fm-Gh* and *Fm-Gci*) overlaying the gravel unit (*Gcm*), and loess (*Ls*) contains phyllites. Regional geomorphic environments cause these different lithofacies and sequences.

Ages of the lacustrine deposits of Taiping T1 (9.46±0.99 ka) and Tuanjie T5 (10.36±0.61 ka), as well as Taiping T3 (9.93±0.75 ka) and Tuanjie T7 (9.98±0.77 ka) (Table. 3), are similar, which confirms from a chronological perspective that the two terraces correspond to each other (Fig. 5).

5.4 Formation and outburst of palaeo-dam

The triangle formed by Tuanjie and the localities of Jiaochang and Xiaohaizi lies around the center of the ancient dammed lake. Outburst sediments are present downstream around the location of Xiaoguanzi-Manaoding (Fig. 1b). Combined with the lithofacies and chronological framework in the Tuanjie terraces, the palaeo-dam has experienced multiple events of damming and dam-breaking. We used the ages of lacustrine deposits, combined with the previous dating results, to classify the blocking and outburst phases of the palaeo-dam.

The palaeo-landslide dam blocked the river before 32.40±2.07 ka (Phase I, 32 ka), as supported by Wang et al. (2012) and Wang et al. (2017): (1) The bottom lacustrine deposits of the palaeo-dammed lake were deposited at 35.13±0.29 cal. ka BP. (2) The palaeo-dammed lake and palaeo-dam boundary in Xiaoguanzi was deposited at 34.87±0.76 and 35.54±0.83 cal. ka BP. (3) Accumulation deposits of a palaeo-dam in Manaoding were deposited at 34.54±0.16 cal. ka BP.

After the first dammed lake phase, the first outburst occurred at 27.11±0.18 ka (Phase II, 27 ka), as evidenced by the deposition of outburst sediments downstream at 27.30±2.80 ka (Ma et al., 2018). Additionally, the presence of deformed layers in the Shawan section (26.5-24.1 ka; Wang et al., 2011; Wang et al., 2012), and the convolution structure in Haizipo (27.74±0.47 ka; Wang et al., 2012), confirm that there had a disaster event occurred around 27.11±0.18 ka. Furthermore, the discovery of the palaeo-landslide in Qiangyangqiao (26.54±0.53 ka, 27.28±0.41 ka; Wang et al., 2012), and the palaeo-dammed lake in Maoxian (26.81±0.98 ka; Wang et al., 2007), suggests that the upper reaches of the Minjiang River experienced several disastrous events around 27 ka.

Subsequently, the palaeo-dam blocked the river again (Phase III, during 27~17 ka), and the elevation may have reached or exceeded the position of the highest lacustrine deposits in the Taiping Terrace. Around 17 ka, the palaeo-dam was broken (Phase IV, 17 ka), exposing the highest lacustrine deposits of the Taiping Terrace. Besides, the palaeo-landslide in Manaoding occurred at 16.75±0.62 cal. ka BP (Wang et al., 2012), suggesting that an event happened around 17 ka, causing the second outburst event and forming a palaeo-landslide downstream.

As seen from our dating results, the lake level of the palaeo-lake descended from the highest point in the Taiping terrace to the T1 terrace between 10.77±1.19 and 9.46±0.99 ka. Furthermore, between 9.98±0.77 and 10.36±0.61 ka, the lake level descended from the position of T7 to T5 in the Tuanjie Terrace. These findings indicate significant fluctuations in the lake level of the palaeo-dammed lake at around 10 ka, suggesting a third dam outburst during this period (Phase V, ~10 ka). The third outburst event can be attributed to a progressive failure of the palaeo-dam. Additionally, the fluctuation in the lake level of the palaeo-lake at around 10 ka is also evident in the Taiping, Shawan, and Tuanjie profiles (Zhong, 2017). Subsequently, the dam body stabilized until the occurrence of the fourth dam break event around 9 ka (Phase VI), leading to the formation of the present riverbed.

About 30 ka BP, during the last glacial period, the formation of Tuanjie Terrace may have been influenced by tectonic activities (such as earthquakes) and climate changes (Shen, 2014; Wang, 2009; Luo et al., 2019; Wang et al., 2012). To better understand the constraints of tectonic activities, climate changes, and the evolution of the palaeo-dam on terrace formation, we discuss the effects of these three factors below.

5.5 The formation and evolution mechanisms of terraces

Numerous studies stated that tectonic activities and climate changes play essential roles in the generation of mountainous terrace and landscape evolution (Maddy et al., 2005; Burgette et al., 2017; Chen et al., 2020; Gao et al., 2020; Narzary et al., 2022; Ma et al., 2023). More recently, researchers have also considered the impact of disaster events (Wang et al., 2021a; Yu et al., 2021). In the Diexi area, the substantial thickness (>200 m) of lacustrine deposits and the multiple loess-paleosol sequences, suggest that tectonic uplift, climate fluctuations, and the effects of damming event influence terraces. Here, we discuss the impact of these three factors on the Tuanjie and Taiping terraces.

5.5.1 The reflection of terraces to tectonic activities

Considering the short distance of only 12 km between Tuanjie and Taiping, we regard them as in the same tectonic uplifting background. In Section 5.2, we divided the upper Minjiang River into three parts: the Zhangla to Gonggaling area (upstream of the Diexi area), the Diexi area (Taiping-Tuanjie), and the Maoxian-Wenchuan area (downstream of the Diexi area). During the damming period of the Diexi palaeo-dammed lake (32-10 ka), the incision rates in these three sections ranged from 8.3-85.3 mm/yr, 13.6-198 mm/yr, and 58 mm/yr, respectively, from upstream to downstream (Table. S2). And the Minshan Block, which includes the Minjiang River, has experienced an average uplift rate of 1.5 mm/yr since the Quaternary (Zhou et al., 2000). It can be observed that the incision rates of the upper reaches of the Minjiang River during the period of 32-10 ka are significantly higher than the uplift rate of the Minshan Block, indicating that tectonic activity has little influence on the formation of regional terraces. In particular, the Taiping-Tuanjie region has a higher incision rate than the upstream and downstream areas, highlighting its unique characteristics. That is, tectonic activity is not a critical factor in the evolution of Tuanjie and Taiping terraces.

5.5.2 Climate fluctuations affected the formation of terraces

Diexi has undergone three transitions from cold and dry to warm and humid climates during 40.5-30.0 ka (Zhang et al., 2009). Particularly, during the period of 30-15 ka, Diexi experienced ten distinguishable climatic and environmental periods (Wang et al., 2014). Furthermore, there were seven alternating periods between cold and warm from 22 to 10 ka (Wang, 2009). In the Zhangla Basin, the climate was cold from 35 to 20 ka, but it changed from cold to warm during 20-10 ka (Zhu, 2014). Tuanjie had a similar climate trend to the Zhangla Basin during 20-10 ka, and Diexi has been subject to frequent climate fluctuations since 40 ka.

The chronological results range from 32.40±2.07 ka to 3.78±0.18 ka. We compared our dating ages with the variations in the climate curves (Fig. 7). Curves a, b, c, and d respectively represent the $\delta^{18}O$ of the Sanbao Cave, the Hulu Cave, the East Asian Monsoon, and the GISP 2 $\delta^{18}O$ record. These four curves show significant fluctuations from the end of the Last Glacial Maximum (LGM) to the early Holocene,

followed by an abrupt change upon entering the Holocene. The two gravel units are older than the lacustrine deposits of the terraces in which they are located, indicating that the input of materials from the upper reaches of the Minjiang River did not cease during the blockage of the palaeo-dam, resulting in the accumulation of such a thick unit of gravels. The loess unit of T5 was deposited at the beginning of the Younger Dryas and after the warm period, reflecting a cold depositional environment. Most paleosol units were deposited in the early Holocene, consistent with indicative warming conditions. Thus, climate change appeared to have a more significant impact on eolian sediments than on terrace formation.

The first two dam-break events (27.11±0.18 and 17.15±0.18 ka) are unrelated to climate change, while the third and fourth outburst events (~10 and ~9 ka) occurred during warm and humid climates. This indicates that the evolution of the terrace accelerated during the early Holocene period. Although the dam-break events became more frequent during the early Holocene, it is challenging to confirm whether warmer periods triggered increased rainfall, leading to the overtopping of the dam, and the formation of terraces. The lack of high-resolution rainfall data makes it difficult to determine the specific influence of climate on terrace formation.

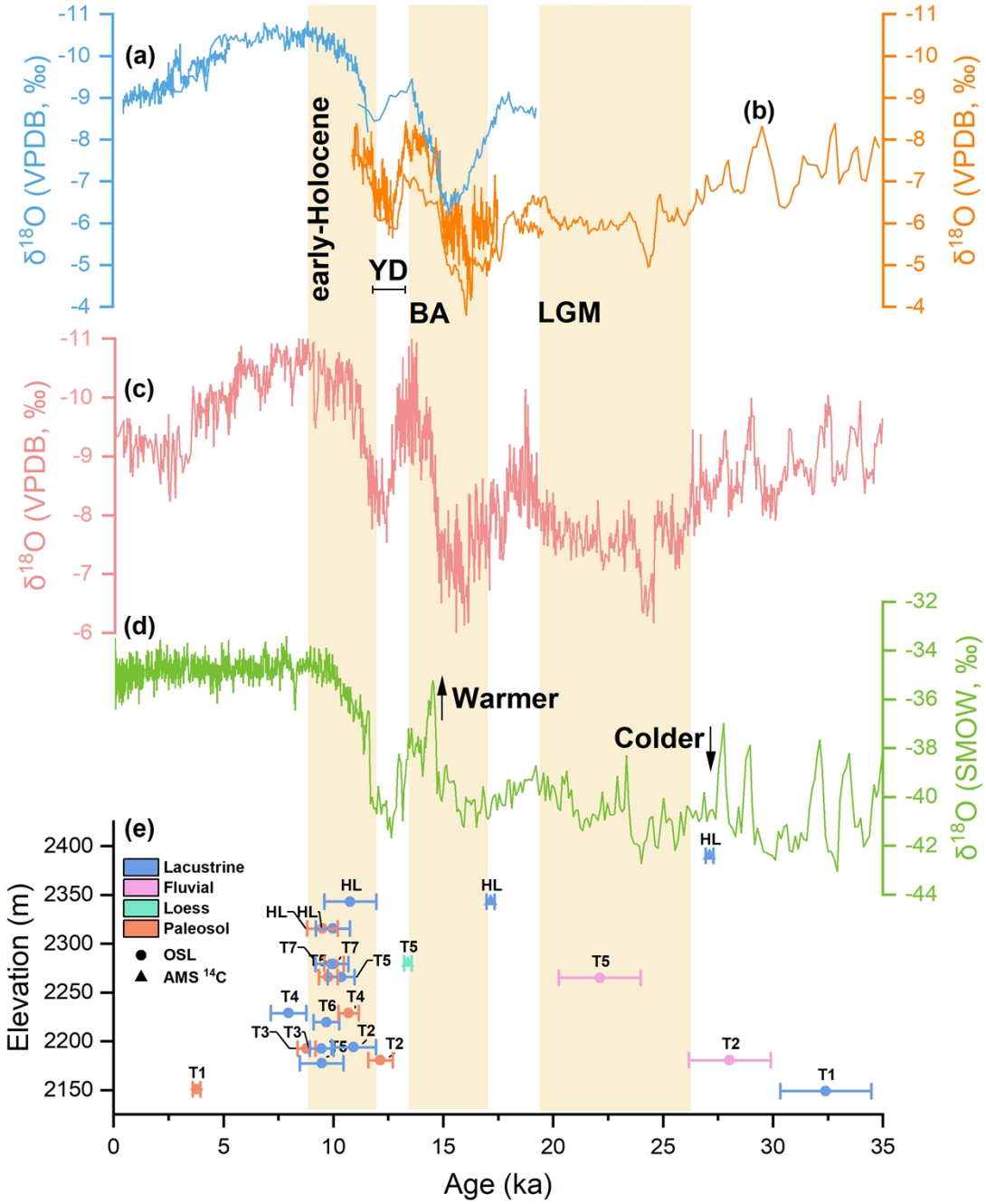

Figure 7. Palaeoclimate records compared with the Diexi OSL and AMS ^{14}C-based terrace chronology. (a) Sanbao Cave (from Wang et al., 2008). (b) δ^{18}O of Hulu Cave (from Wang et al., 2001). (c) East Asian Monsoon (from Cheng et al., 2016). (d) GISP 2 δ^{18}O record (from Grootes et al., 1993). (e) Ages of each unit of the Tuanjie and Taiping Terraces. The vertical-orange bars in the figure show the duration of the early Holocene, the Bølling-Allerød interstadial, and the LGM. The YD is located between the early Holocene and Bølling-Allerød interstadial.

However, climate change can affect the topography of terrace staircases. Tuanjie Terrace T2 has an irregular age-depth sequence, indicating repeated fluctuations in the lake level by 11 meters during the period of 18.60±2.86~10.63±1.27 ka (Table. S2) (ages dated by Mao, 2011; Jiang et al., 2014; Shi, 2020).

This suggests that the geomorphological features of Tuanjie Terrace T1 and T2 have been influenced by climate change. The repetitive long-term wave erosion, fluctuating along the palaeo-lake level, resulted in the beveling and backwearing of T2 (Malatesta et al., 2021). As a result, Tuanjie T1 has the widest terrace surface (Fig. 7).

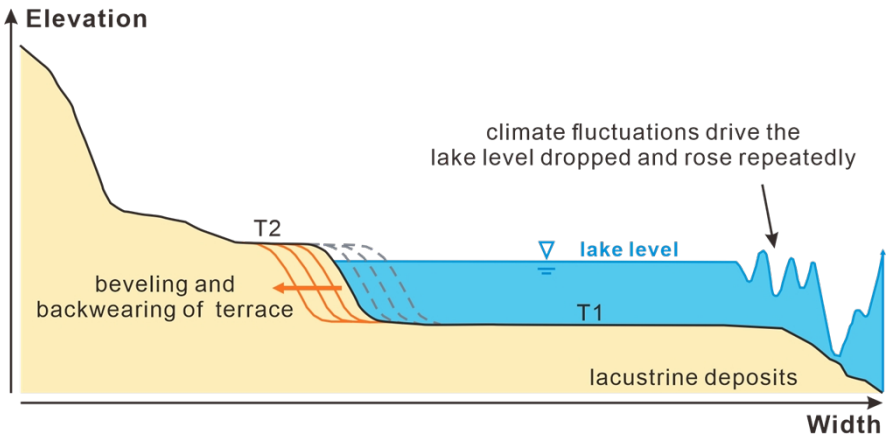

Figure 8. Climate fluctuations drive the landscape evolution of the Tuanjie Terrace T1 and T2 (modified from Malatesta et al., 2021). Repeated drops and rises of the lake level are influenced by climate change, resulting in beveling and backwearing of the terrace, and the widest surface of T1.

5.5.3 The instability of the palaeo-dam

Damming and outburst events can strongly impact upstream and downstream areas, causing aggradation and incision (Fig. 9) (Hewitt et al., 2008; Korup and Montgomery, 2008). The upstream and downstream effects of the blockage are a rapid rise in water level followed by potential upstream flooding (Guo et al., 2016). The upstream sediment accumulation can abrade and protect the channel bedrock, significantly affecting river evolution and regional landscapes (Korup et al., 2010; Yu et al., 2021). During the blockage period, the dam impedes the river and maintains its base level. Gravity and density cause the material to be deposited in the Diexi palaeo-dammed lake, forming a channel. During the outburst period, the lake level drops, and the river cuts through the sediments, forming terraces along the river. Each outburst event does not result in a complete breach of the palaeo-dam, so the river channel cuts down through the terraces after each breach (Wang et al., 2012). Subsequently, the downstream channel restarts, forming a new, narrow, steep valley (Wang et al., 2021a).

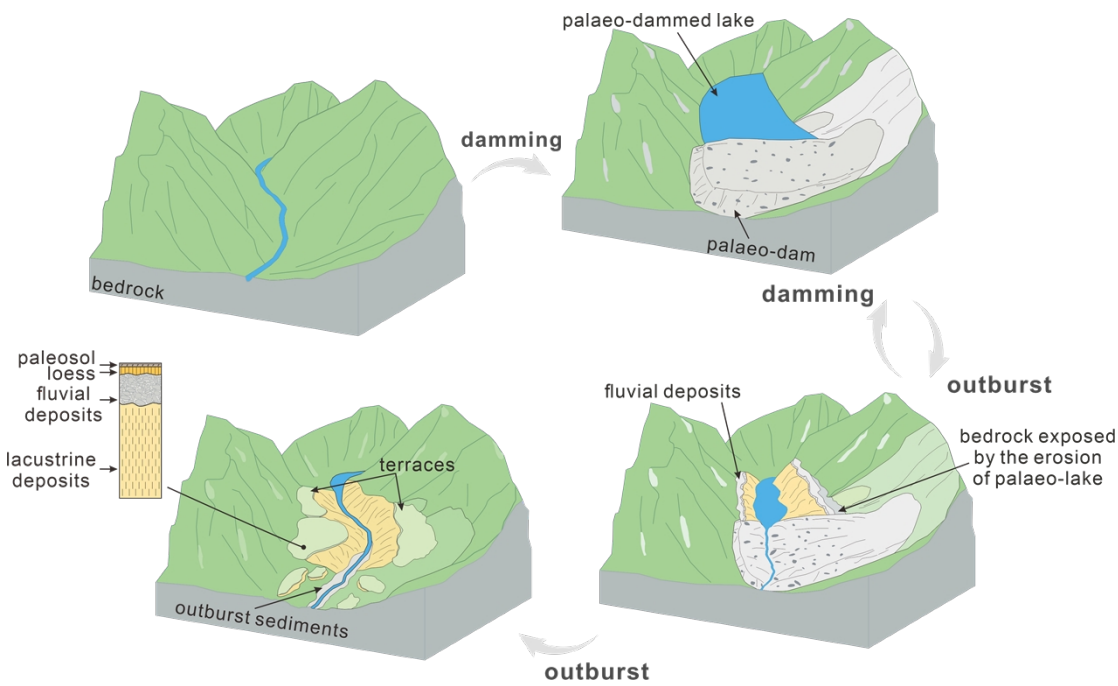

Figure 9. Model of palaeo-landslide dam driven valley landscape and terrace evolution. The palaeo-landslide blocked the river and formed a palaeo-dam, the water level rose and formed a palaeo-dammed lake. During the outburst period, the palaeo-dammed lake shrank, the lacustrine and fluvial deposits were exposed, and the palaeo-dam was cut down to form a river channel. Subsequently, through repeated damming and outbursts, the palaeo-dam completely collapsed and deposited as outburst sediments, and terraces were formed along the river. The stratigraphical sequence of the terrace is lacustrine deposits, fluvial deposits, loess, and paleosol, from bottom to top.

Most lacustrine deposits in the Tuanjie and Taiping Terraces were deposited from 32.40 ±2.07 ka to 7.97±0.81 ka. We propose that repeated blockages and outbursts of the palaeo-dam caused these depositions. Initially, the palaeo-dam had a large blocking scale, resulting in a high lake level, and corresponding lacustrine deposits at higher positions with older age. Since the palaeo-dam gradually broke, the height of the palaeo-dam body decreased, leading to a drop in the lake surface and the formation of lower staircases with younger ages, such as the age of the highest lacustrine deposits older than Tuanjie T2-T7. Besides, the downcutting rate of Tuanjie T7 to Tuanjie T5 (1652.33 mm/a) is higher than the maximum channel incision rate (198.00 mm/a) of the study area around 10 ka ago (Duan et al., 2002). This rapid downcutting supports that the damming and dam-breaking of the palaeo-dam are critical factors in the formation and evolution of the Diexi terraces.

As terraces developed near the palaeo-dam are considered to be remnants of the dam itself (Zhang et al., 2013; Yu et al., 2021), the Tuanjie terraces reflect that the Diexi palaeo-dammed lake experienced several outbursts before its extinction, with each terrace corresponding to an outburst event (Duan et al.,

2002; Wang, 2009; Wang et al., 2020a). The interval between each outburst is about 1500 years (Wang et al., 2007). Our dating results support that the Diexi palaeo-landslide dam had multiple dam-breaking events, as mentioned in Section 5.4. During 32.40±2.07 ka, the height of the dam body reached at least the highest lacustrine deposits of the Tuanjie Terrace. The age of the fluvial deposits in Tuanjie T2 (28.03±1.86 ka) is similar to that of the outburst sediments (~27.3±2.8 ka, Ma et al., 2018), indicating the occurrence of the first outburst event around 27 ka. This event caused the lake level to drop to the surface of the Tuanjie T2, accompanied by the input of upstream gravels deposited at the T2 position. The ages of the loess and paleosol, ranging from 13.38±0.08 to 3.78±0.18 ka, support the idea that loess and paleosol were deposited after the third outburst event.

The evolution of each terrace and paleo-dam can be summarized as follows: Before 32 ka, a palaeo-dam blocked the river, with its tip reaching 2500 m (Fig. 10a). Around 27 ka ago, the palaeo-dam burst open, exposing the Tunajie T2 and the highest lacustrine deposits of Tuanjie (Fig. 10b). Subsequently, the palaeo-dam blocked the river again between 27 and 17 ka ago. During this period, the lake shore receded until the Taiping Terrace (Fig. 10c). The second palaeo-dam outburst occurred 17 ka ago, exposing the highest lacustrine deposits of Taiping (Fig. 10d). Tunajie T7 to T5 formed during the third dam-breaking, which took place around 10 ka, and was a progressive outburst event (Fig. 10e). Finally, during the fourth outburst approximately 9 ka ago, Tuanjie T4, T3 and T1 terraces formed, and eolian sediments were deposited during this period (Fig. 10f).

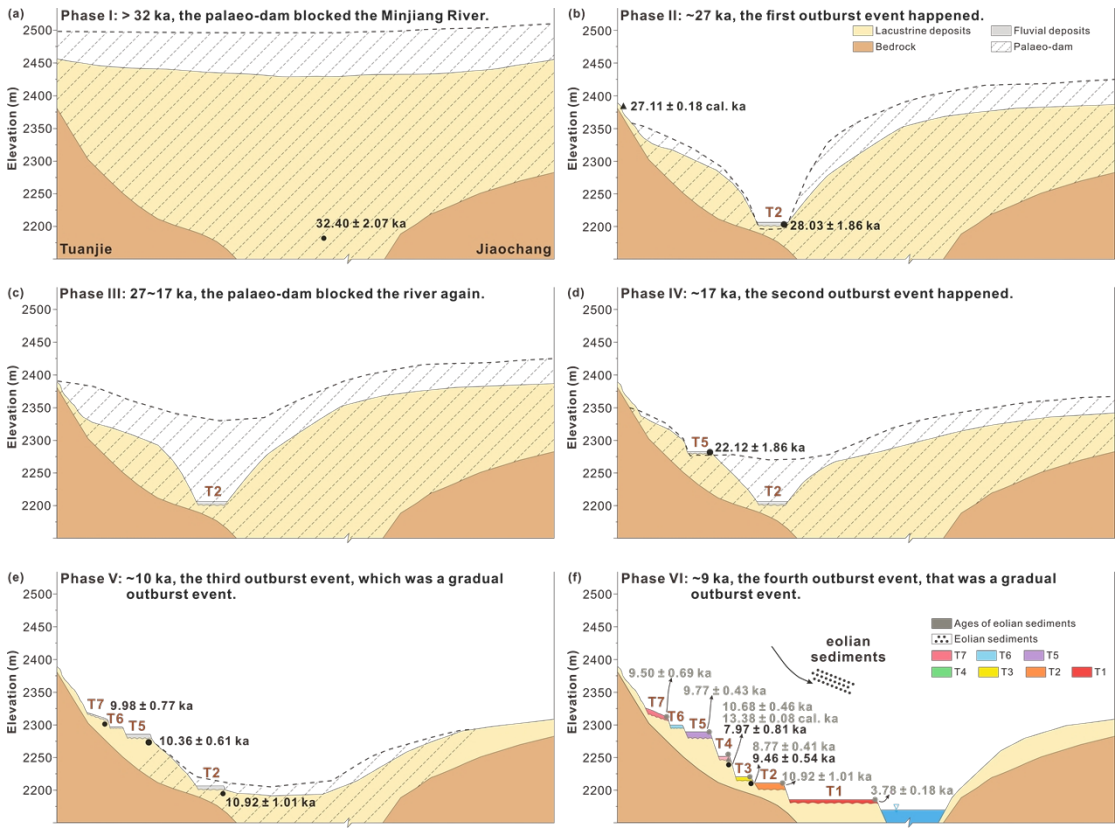

Figure 10. Schematic evolution and the relationship between palaeo-landslide dam and Tuanjie Terrace. (a) Before 32 ka, the palaeo-dam blocked the Minjiang River, and lacustrine sediments were deposited. (b) The first outburst event happened at ~27 ka. The lake level dropped to the surface of Tuanjie T2, and the input of upstream gravels was deposited at the T2 position. During this period, the lacustrine deposits of T2 and the highest positions were exposed. (c) The palaeo-dam blocked the river again at 27~17 ka, the palaeo-lake shore receded till the Taiping. (d) The second outburst event happened at ~17 ka, and the highest lacustrine deposits of Taiping Terraces were exposed. (e) The third outburst occurred at ~10 ka, a progressive outburst event. Terrace T7, T6, and T5 were formed during the third dam-breaking event. Terrace T2 was influenced by the repeatedly dropped and rose of palaeo-lake level during this period, as discussed in Fig. 8. (f) The fourth outburst event, a progressive outburst event, happened at ~9 ka. Terraces T4, T3, and T1 were exposed, and eolian sediments were deposited during this period. The detailed ages are shown in Fig. 5.

6 Conclusions

The Tuanjie and Taiping Terraces have a similar stratigraphic sequence, characterized by a base of lacustrine deposits, overlain by gravels, loess, and paleosol. The Minjiang River has transported the gravel of the Tuanjie terraces, whereas the Luobogou Gully influences the gravel in the Taiping terraces. Two sequences of mud-clast layers in the Taiping T3 terrace imply that damming events control the formation of the T3 terrace.

Combining geomorphology, sedimentology, and chronology reveals that Taiping terraces T1 to T3

correspond to Tuanjie T5 to T7. Tectonic movements and climate fluctuations are not the primary factors influencing terrace formation; instead, damming and outburst events play a crucial role. Two damming and four outburst events have been identified. Before 32 ka, the river was blocked, causing the lake level to rise to its highest recorded level based on lacustrine deposits. The dam remained intact until 27 ka, when the first outburst event happened. During this event, the height of the palaeo-dam dropped to near the surface of Tuanjie T2. The palaeo-dam blocked the river again between 27 and 17 ka, allowing the lake surface to extend toward the Taiping Terrace. Another outburst event occurred around 17 ka, exposing the highest lacustrine deposits. Tuanjie T7 to T5 corresponds to the third dam-breaking period, which occurred approximately 10 ka ago as a progressive outburst event. Tuanjie T4, T3, and T1 are associated with the fourth progressive collapse event around 9 ka.

This finding has important implications for revealing the formation and evolution of the Diexi palaeo-landslide dammed lake. It provides crucial knowledge that contributes to understanding the formation and evolution of these terraces and reconstructing the evolution of the Diexi palaeo-landslide dam. This study proposes a new perspective on terrace formation in the eastern margin of the Tibetan Plateau, which can enhance our understanding of the impact of landslide dams on fluvial evolution. Additionally, it holds important implications in studying the evolution of palaeo-climate and palaeo-environment, providing insight into future mountainous engineering projects.

Author contributions

JL wrote the manuscript and analyzed the data. XF and ZD discussed the results and provided guidance and funding. SK conducted OSL dating, ML polished the language.

Competing interests

An author is a member of the editorial board of the journal Earth Surface Dynamics. The peer-review process was guided by an independent editor, and the authors have also no other competing interest to declare.

Acknowledgments

We thank Lanxin Dai, Chengbin Zou, Yujin Zhong, Binbin Luo, Bing Xia, Kunyong Xiong for fieldwork assistance, and Xiangyang Dou for revising the figures.

Financial support

This research is financially supported by the Funds for National Science Foundation for Outstanding Young Scholars, Grant no. 42125702, the National Natural Science Foundation of China, Grant no. 42207223, the Natural Science Foundation of Sichuan Province, Grant no. 2022NSFSC003, and the State Key Laboratory of Geohazard Prevention and Geoenvironment Protection Independent Research Project, Grant no. SKLGP2021Z025.

References

An, W., Zhao, J., Yan, X., Li, Z., and Su, Z.: Tectonic deformation of lacustrine sediments in qiangyang on the Minjiang fault zone and ancient earthquake, Seismology and Geology, 30, 980-988, https://doi.org/10.3969/j.issn.0253-4967.2008.04.014, 2008.

Avsin, N., Vandenberghe, J., van Balen, R., Kiyak, N. G., and Ozturk, T.: Tectonic and climatic controls on Quaternary fluvial processes and river terrace formation in a Mediterranean setting, the Goksu River, southern Turkey, Quaternary Research, 91, 533-547, https://doi.org/10.1017/qua.2018.129, 2019.

Bell, C. M.: Punctuated drainage of an ice-dammed quaternary lake in southern South America, Geogr Ann A, 90a, 1-17, https://doi.org/10.1111/j.1468-0459.2008.00330.x, 2008.

Burgette, R. J., Weldon, R. J., Abdrakhmatov, K. Y., Ormukov, C., Owen, L. A., and Thompson, S. C.: Timing and process of river and lake terrace formation in the Kyrgyz Tien Shan, Quaternary Science Reviews, 159, 15-34, https://10.1016/j.quascirev.2017.01.003, 2017.

Caputo, R., Salviulo, L., and Bianca, M.: Late Quaternary activity of the Scorciabuoi Fault (southern Italy) as inferred from morphotectonic investigations and numerical modeling, Tectonics, 27, 1-18, https://doi.org/10.1029/2007tc002203, 2008.

Chen, G., Zheng, W., Xiong, J., Zhang, P., Li, Z., Yu, J., Li, X., Wang, Y., and Zhang, Y.: Late Quaternary fluvial landform evolution and controlling factors along the Yulin River on the Northern Tibetan Plateau, Geomorphology, 363, https://doi.org/10.1016/j.geomorph.2020.107213, 2020.

Chen, H. and Li, Y.: River terrace responding to the obduction of the Longmenshan fault zone in the upper Min River basin, Mountain Research, 32, 535-540, https://doi.org/10.16089/j.cnki.1008-2786.2014.05.003, 2014.

Chen, Y., Aitchison, J. C., Zong, Y., and Li, S.-H.: OSL dating of past lake levels for a large dammed lake in southern Tibet and determination of possible controls on lake evolution, Earth Surface Processes and Landforms, 41, 1467-1476, https://10.1002/esp.3907, 2016.

Chen, Z. and Lin, Q.: Significance of neotectonic movement of lake extension and shrinkage in Qinghai-Tibet Plateau, Earthquake, 31-40+52, https://doi.org/CNKI:SUN:DIZN.0.1993-01-006, 1993.

Cheng, H., Edwards, R. L., Sinha, A., Spötl, C., Yi, L., Chen, S., Kelly, M., Kathayat, G., Wang, X., Li, X., Wang, X., Wang, Y., Ning, Y., and Zhang, H.: The Asian monsoon over the past 640,000 years and ice age terminations, Nature, 534, 640-646, https://doi.org/10.1038/nature18591, 2016.

Counts, R. C., Murari, M. K., Owen, L. A., Mahan, S. A., and Greenan, M.: Late Quaternary chronostratigraphic framework of terraces and alluvium along the lower Ohio River, southwestern Indiana and western Kentucky, USA, Quaternary Science Reviews, 110, 72-91, https://doi.org/10.1016/j.quascirev.2014.11.011, 2015.

Dai, L., Fan, X., Jansen, J. D., and Xu, Q.: Landslides and fluvial response to landsliding induced by the 1933 Diexi earthquake, Minjiang River, eastern Tibetan Plateau, Landslides, 18, 3011-3025, https://doi.org/10.1007/s10346-021-01717-2, 2021.

Dai, L., Fan, X., Wang, D., Zhang, F., Yunus, A. P., Subramanian, S. S., Rogers, J. D., and Havenith, H.-B.: Electrical resistivity tomography revealing possible breaching mechanism of a Late Pleistocene long-lasted gigantic rockslide dam in Diexi, China, Landslides, 20, 1449-1463, https://10.1007/s10346-023-02048-0, 2023.

Deevey, E. S., Gross, M. S., Hutchinson, G. E., and Kraybill, H. L.: The natural 14C contents of materials from hard-water lakes, Proceedings of the National Academy of Sciences, 40, 285-288, https://doi.org/10.2307/88928, 1954.

Deng, B., Liu, S., Liu, S., Jansa, L., Li, Z., and Zhong, Y.: Progressive Indosinian N-S deformation of the Jiaochang structure in the Songpan-Ganzi fold-belt, Western China, PLoS One, 8, e76732, https://doi.org/10.1371/journal.pone.0076732, 2013.

do Prado, A. H., de Almeida, R. P., Galeazzi, C. P., Sacek, V., and Schlunegger, F.: Climate changes and the formation of fluvial terraces in central Amazonia inferred from landscape evolution modeling, Earth Surf Dynam, 10, 457-471, https://doi.org/10.5194/esurf-10-457-2022, 2022.

Duan, L.: The ancient barrier lake and geoenvironment, Diexi, Minjiang River, Chengdu University of Technology, Chengdu, 65 pp., 2002.

Duan, L., Wang, L., Yang, L., and Dong, X.: The ancient climatic evolution characteristic reflected by carbon and oxygen isotopes of carbonate in the ancient barrier lacustrine deposits, Diexi, Minjiang River, The Chinese Journal of Geological Hazard and Control, 13, 91-96, https://doi.org/10.3969/j.issn.1003-8035.2002.02.019, 2002.

Duller, G. A. T.: Distinguishing quartz and feldspar in single grain luminescence

measurements, Radiation Measurements, 37, 161-165, https://10.1016/s1350-4487(02)00170-1, 2003.
Durcan, J. A., King, G. E., and Duller, G. A. T.: DRAC: Dose Rate and Age Calculator for trapped charge dating, Quaternary Geochronology, 28, 54-61, https://10.1016/j.quageo.2015.03.012, 2015.
Fan, X., Dai, L., Zhong, Y., Jingjuan, L., and Wang, L.: Recent research on the Diexi paleo-landslide: dam and lacustrine deposits upstream of the Minjiang River, Sichuan, China, Earth Science Frontiers, 28, 71-84, https://doi.org/10.13745/j.esf.sf.2020.9.2, 2021.
Fan, X., Xu, Q., van Westen, C. J., Huang, R., and Tang, R.: Characteristics and classification of landslide dams associated with the 2008 Wenchuan earthquake, Geoenvironmental Disasters, 4, 1-15, https://doi.org/10.1186/s40677-017-0079-8, 2017.
Fan, X., Yunus, A. P., Jansen, J. D., Dai, L., Strom, A., and Xu, Q.: Comment on 'Gigantic rockslides induced by fluvial incision in the Diexi area along the eastern margin of the Tibetan Plateau' by Zhao et al. (2019) Geomorphology 338, 27–42, Geomorphology, 402, https://doi.org/10.1016/j.geomorph.2019.106963, 2019.
Fan, X., Scaringi, G., Xu, Q., Zhan, W., Dai, L., Li, Y., Pei, X., Yang, Q., and Huang, R.: Coseismic landslides triggered by the 8th August 2017 Ms 7.0 Jiuzhaigou earthquake (Sichuan, China): factors controlling their spatial distribution and implications for the seismogenic blind fault identification, Landslides, 15, 967-983, https://doi.org/10.1007/s10346-018-0960-x, 2018.
Gao, H. S., Li, Z. M., Liu, F. L., Wu, Y. J., Li, P., Zhao, X., Li, F. Q., Guo, J., Liu, C. R., Pan, B. T., and Jia, H. T.: Terrace formation and river valley development along the lower Taohe River in central China, Geomorphology, 348, https://doi.org/10.1016/j.geomorph.2019.106885, 2020.
Gao, X. and Li, Y.: Comparison on the incision rate in the upper and middle reaches of Minjiang River, Resources and environment in the Yangtze Basin, 15, 517-521, https://doi.org/10.3969/j.issn.1004-8227.2006.04.020, 2006.
Giano, S. I. and Giannandrea, P.: Late Pleistocene differential uplift inferred from the analysis of fluvial terraces (southern Apennines, Italy), Geomorphology, 217, 89-105, https://doi.org/10.1016/j.geomorph.2014.04.016, 2014.
Gorum, T., Fan, X., van Westen, C. J., Huang, R. Q., Xu, Q., Tang, C., and Wang, G.: Distribution pattern of earthquake-induced landslides triggered by the 12 May 2008 Wenchuan earthquake, Geomorphology, 133, 152-167, https://doi.org/10.1016/j.geomorph.2010.12.030, 2011.
Grootes, P. M., Stulver, M., White, J. W. C., Johnsen, S. J., and Jouzel, J.: Comparison of oxygen records from the GISP2 and GRIP Greenland ice cores, Nature, 366, 6455, https://doi.org/10.1038/366552a0, 1993.
Guo, P.: Grain Size Characteristics and Optically stimulated luminescence Geochronology of Sediments in Diexi palaeo-dammed Lake, Upper Reaches of Minjiang River, China University of Geosciences, Beijing, 85 pp., 2018.
Guo, X., Sun, Z., Lai, Z., Lu, Y., and Li, X.: Optical dating of landslide-dammed lake deposits in the upper Yellow River, Qinghai-Tibetan Plateau, China, Quaternary

International, 392, 233-238, https://doi.org/10.1016/j.quaint.2015.06.021, 2016.
Hewitt, K., Clague, J. J., and Orwin, J. F.: Legacies of catastrophic rock slope failures in mountain landscapes, Earth-Science Reviews, 87, 1-38, https://doi.org/10.1016/j.earscirev.2007.10.002, 2008.
Hewitt, K., Gosse, J., and Clague, J. J.: Rock avalanches and the pace of late Quaternary development of river valleys in the Karakoram Himalaya, Geological Society of America Bulletin, 123, 1836-1850, https://doi.org/10.1130/b30341.1, 2011.
Hou, Z., Li, Z., Qu, X., Gao, Y., Hua, L., Zheng, M., Li, S., and Yuan, W.: The uplift process of the Qinghai-Tibet Plateau since 0.5Ma - Evidence from hot water activity in the Gangdese belt, Science in China, 31, 27-33, 2001.
Hu, H.-P., Feng, J.-L., and Chen, F.: Sedimentary records of a palaeo-lake in the middle Yarlung Tsangpo: Implications for terrace genesis and outburst flooding, Quaternary Science Reviews, 192, 135-148, https://10.1016/j.quascirev.2018.05.037, 2018.
Huang, Z., Tang, R., and Liu, S.: Re-discussion on the Jiaochang Arcuate Structure, Sichuan Province, and the Seismogenic Structure for Diexi Earthquake in 1933, Earthquake Research in China, 17, 51-62, https://doi.org/CNKI:SUN:ZDZW.0.2003-01-005, 2003.
Jiang, H., Zhong, N., Li, Y., Xu, H., Yang, H., and Peng, X.: Soft sediment deformation structures in the Lixian lacustrine sediments, eastern Tibetan Plateau and implications for postglacial seismic activity, Sedimentary Geology, 344, 123-134, https://doi.org/10.1016/j.sedgeo.2016.06.011, 2016.
Jiang, H., Mao, X., Xu, H., Yang, H., Ma, X., Zhong, N., and Li, Y.: Provenance and earthquake signature of the last deglacial Xinmocun lacustrine sediments at Diexi, East Tibet, Geomorphology, 204, 518-531, https://doi.org/10.1016/j.geomorph.2013.08.032, 2014.
Kang, S., Wang, X., and Lu, Y.: Quartz OSL chronology and dust accumulation rate changes since the Last Glacial at Weinan on the southeastern Chinese Loess Plateau, Boreas, 42, 815-829, https://10.1111/bor.12005, 2013.
Kang, S., Du, J., Wang, N., Dong, J., Wang, D., Wang, X., Qiang, X., and Song, Y.: Early Holocene weakening and mid- to late Holocene strengthening of the East Asian winter monsoon, Geology, 48, 1043-1047, https://10.1130/g47621.1, 2020.
Kaplan, M. R., Wolfe, A. P., and Miller, G. H.: Holocene Environmental Variability in Southern Greenland Inferred from Lake Sediments, Quaternary Research, 58, 149-159, https://doi.org/10.1006/qres.2002.2352, 2017.
Kirby, E., Whipple, K. X., Burchfiel, B. C., Tang, W., Berger, G., Sun, Z., and Chen, Z.: Neotectonics of the Min Shan, China：Implications for mechanisms driving Quaternary deformation along the eastern margin of the Tibetan Plateau, Geological Society of America Bulletin, 112, 375-393, https://doi.org/10.1130/0016-7606(2000)112<375:NOTMSC>2.0.CO;2, 2000.
Korup, O. and Montgomery, D. R.: Tibetan plateau river incision inhibited by glacial stabilization of the Tsangpo gorge, Nature, 455, 786-789, https://doi.org/10.1038/nature07322, 2008.
Korup, O., Densmore, A. L., and Schlunegger, F.: The role of landslides in mountain

range evolution, Geomorphology, 120, 77-90, https://doi.org/10.1016/j.geomorph.2009.09.017, 2010.
Korup, O., Clague, J. J., Hermanns, R. L., Hewitt, K., Strom, A. L., and Weidinger, J. T.: Giant landslides, topography, and erosion, Earth and Planetary Science Letters, 261, 578-589, https://doi.org/10.1016/j.epsl.2007.07.025, 2007.
Krivonogov, S. K., Takahara, H., Kuzmin, Y. V., Orlova, L. A., Timothy Jull, A. J., Nakamura, T., Miyoshi, N., Kawamuro, K., and Bezrukova, E. V.: Radiocarbon Chronology of the Late Pleistocene–Holocene Paleogeographic Events in Lake Baikal Region (Siberia), Radiocarbon, 46, 745-754, https://doi.org/10.1017/s0033822200035785, 2016.
Li, J. and Fang, X.: Study on the uplift and environmental change of the Qinghai-Tibet Plateau, Chinese Science Bulletin, 43, 1563-1574, https://doi.org/CNKI:SUN:KXTB.0.1998-15-000, 1998.
Liu, Y., Wang, X., Su, Q., Yi, S., Miao, X., Li, Y., and Lu, H.: Late Quaternary terrace formation from knickpoint propagation in the headwaters of the Yellow River, NE Tibetan Plateau, Earth Surface Processes and Landforms, 46, 2788-2806, https://doi.org/10.1002/esp.5208, 2021.
Lu, H., An, Z., Wang, X., Tan, H., Zhu, R., Ma, H., Li, Zhen, Miao, X., and Wang, X.: The staged uplift of the northeastern margin of the Qinghai-Tibet Plateau in the recent 14 Ma Geomorphic evidence, Science in China Series D Earth Sciences, 34, 855-864, https://doi.org/10.3321/j.issn:1006-9267.2004.09.008, 2004.
Luo, X., Yin, Z., and Yang, L.: Preliminary analysis on the development characteristics of river terraces and their relationship with ancient landslides in the upper reaches of Minjiang River, Quaternary Sciences, 39, 391-398, https://doi.org/10.11928/j.issn.1001-7410.2019.02.11, 2019.
Ma, J.: Sedimentary Characteristics of Outburst Deposits and Inversion of Outburst Flood Induced by the Diexi Paleo Dammed Lake of the Upper Minjiang River in China, China University of Geosciences, Beijing, 97 pp., 2017.
Ma, J., Chen, J., Cui, Z., Zhou, W., Liu, C., Guo, P., and Shi, Q.: Sedimentary evidence of outburst deposits induced by the Diexi paleolandslide-dammed lake of the upper Minjiang River in China, Quaternary International, 464, 460-481, https://doi.org/10.1016/j.quaint.2017.09.022, 2018.
Ma, Z., Peng, T., Feng, Z., Li, X., Song, C., Wang, Q., Tian, W., and Zhao, X.: Tectonic and climate controls on river terrace formation on the northeastern Tibetan Plateau: Evidence from a terrace record of the Huangshui River, Quaternary International, 656, 16-25, https://10.1016/j.quaint.2022.11.004, 2023.
Maddy, D., Demir, T., Bridgland, D. R., Veldkamp, A., Stemerdink, C., van der Schriek, T., and Westaway, R.: An obliquity-controlled Early Pleistocene river terrace record from Western Turkey?, Quaternary Research, 63, 339-346, https://10.1016/j.yqres.2005.01.004, 2005.
Malatesta, L. C., Finnegan, N. J., Huppert, K. L., and Carreño, E. I.: The influence of rock uplift rate on the formation and preservation of individual marine terraces during multiple sea-level stands, Geology, 50, 101-105, https://doi.org/10.1130/g49245.1, 2021.

Mao, X.: Preliminary study on lacustrine sediments at Diexi in the upper reach of the Minjiang River during the last deglaciation, China university of Geosciences, Beijing, 71 pp., 2011.
Miall, A. D.: Principles Of Sedimentary Basin, Springer, 616 pp.2000.
Molnar, P. and Houseman, G. A.: Rayleigh-Taylor instability, lithospheric dynamics, surface topography at convergent mountain belts, and gravity anomalies, Journal of Geophysical Research: Solid Earth, 118, 2544-2557, https://doi.org/10.1002/jgrb.50203, 2013.
Molnar, P., England, P., and Martinod, J.: Mantle dynamics, uplift of the Tibetan Plateau, and the Indian monsoon, Journal of Geophysical Research: Solid Earth, 118, 2544-2557, https://doi.org/10.1029/93RG02030, 1993.
Montgomery, D. R., Hallet, B., Yuping, L., Finnegan, N., Anders, A., Gillespie, A., and Greenberg, H. M.: Evidence for Holocene megafloods down the tsangpo River gorge, Southeastern Tibet, Quaternary Research, 62, 201-207, https://10.1016/j.yqres.2004.06.008, 2004.
Murray, A. S. and Wintle, A. G.: Luminescence dating of quartz using an improved single-aliquot regenerative-dose protocol, Radiation Measurements, 32, 57-73, https://doi.org/10.1016/S1350-4487(99)00253-X, 2000.
Narzary, B., Singh, A. K., Malik, S., Mahadev, and Jaiswal, M. K.: Luminescence chronology of the Sankosh river terraces in the Assam-Bhutan foothills of the Himalayas: Implications to climate and tectonics, Quaternary Geochronology, 72, https://10.1016/j.quageo.2022.101364, 2022.
Oh, J. S., Seong, Y. B., Hong, S., and Yu, B. Y.: Paleo-shoreline changes in moraine dammed lake Khagiin Khar, Khentey Mountains, Central Mongolia, Journal of Mountain Science, 16, 1215-1230, https://doi.org/10.1007/s11629-019-5445-4, 2019.
Okuno, J., Nakada, M., Ishii, M., and Miura, H.: Vertical tectonic crustal movements along the Japanese coastlines inferred from late Quaternary and recent relative sea-level changes, Quaternary Science Reviews, 91, 42-61, https://doi.org/10.1016/j.quascirev.2014.03.010, 2014.
Pan, B., Burbank, D., Wang, Y., Wu, G., Li, J., and Guan, Q.: A 900 k.y. record of strath terrace formation during glacial-interglacial transitions in northwest China, Geology, 31, https://doi.org/10.1130/g19685.1, 2003.
Pan, B., Hu, X., Gao, H., Hu, Z., Cao, B., Geng, H., and Li, Q.: Late Quaternary river incision rates and rock uplift pattern of the eastern Qilian Shan Mountain, China, Geomorphology, 184, 84-97, https://doi.org/10.1016/j.geomorph.2012.11.020, 2013.
Prescott, J. R. and Hutton, J. T.: Cosmic ray contributions to dose rates for luminescence and ESR dating：large depths and long-term time variations, Radiation Measurements, 23, 497-500, https://10.1016/1350-4487(94)90086-8, 1994.
Rees-Jones, J.: Optical dating of young sediments using fine-grain quartz, Ancient TL, 13, 9-14, 1995.
Reimer, P. J., Austin, W. E. N., Bard, E., Bayliss, A., Blackwell, P. G., Bronk Ramsey, C., Butzin, M., Cheng, H., Edwards, R. L., Friedrich, M., Grootes, P. M., Guilderson, T. P., Hajdas, I., Heaton, T. J., Hogg, A. G., Hughen, K. A., Kromer, B., Manning, S.

W., Muscheler, R., Palmer, J. G., Pearson, C., van der Plicht, J., Reimer, R. W., Richards, D. A., Scott, E. M., Southon, J. R., Turney, C. S. M., Wacker, L., Adolphi, F., Büntgen, U., Capano, M., Fahrni, S. M., Fogtmann-Schulz, A., Friedrich, R., Köhler, P., Kudsk, S., Miyake, F., Olsen, J., Reinig, F., Sakamoto, M., Sookdeo, A., and Talamo, S.: The IntCal20 Northern Hemisphere Radiocarbon Age Calibration Curve (0–55 cal kBP), Radiocarbon, 62, 725-757, https://doi.org/10.1017/rdc.2020.41, 2020.

Schumm, S. A. and Parker, R. S.: Implications of Complex Response of Drainage Systems for Quaternary Alluvial Stratigraphy, Nature, 243, 99-100, https://doi.org/10.1038/physci243099a0, 1973.

Shen, M.: Earthquake Information Study For Paleo-dammed Lake At Minjiang River Upstream, Chengdu University of Technology, Chengdu, 1-129 pp., 2014.

Shi, W.: Impact of tectonic activities and climate change on the lacustrine sediments in the eastern Tibet during the last deglaciation, Institute of Geology, China Earthquake Administrator, Beijing, 135 pp., 2020.

Shi, Y., Li, J., Li, B., Yao, T., Wang, S., Li, S., Cui, Z., Wang, F., Pan, B., Fang, X., and Zhang, Q.: Uplift of the Qinghai—Xizang (Tibetan) Plateau and east Asia environmental change during late cenozoic, ACTA GEOGRAPHICA SINICA, 12-22, https://doi.org/10.3321/j.issn:0375-5444.1999.01.002, 1999.

Singh, A. K., Pattanaik, J. K., Gagan, and Jaiswal, M. K.: Late Quaternary evolution of Tista River terraces in Darjeeling-Sikkim-Tibet wedge: Implications to climate and tectonics, Quaternary International, 443, 132-142, https://doi.org/10.1016/j.quaint.2016.10.004, 2017.

Srivastava, P., Tripathi, J. K., Islam, R., and Jaiswal, M. K.: Fashion and phases of late Pleistocene aggradation and incision in the Alaknanda River Valley, western Himalaya, India, Quaternary Research, 70, 68-80, https://doi.org/10.1016/j.yqres.2008.03.009, 2017.

Tang, R., Jiang, N., and Liu, S.: Recognition of the Geological Setting and the Seismogenic Condition for the Diexi Magnitude 7.5 Earthquake, Journal of seisnological research, 6, 327-338, https://doi.org/CNKI:SUN:DZYJ.0.1983-03-011, 1983.

Vásquez, A., Flores-Aqueveque, V., Sagredo, E., Hevia, R., Villa-Martínez, R., Moreno, P. I., and Antinao, J. L.: Evolution of Glacial Lake Cochrane During the Last Glacial Termination, Central Chilean Patagonia (~47°S), Frontiers in Earth Science, 10, 1-19, https://doi.org/10.3389/feart.2022.817775, 2022.

Wang, H., Wang, P., Hu, G., Ge, Y., and Yuan, R.: An Early Holocene river blockage event on the western boundary of the Namche Barwa Syntaxis, southeastern Tibetan Plateau, Geomorphology, 395, 1-20, https://doi.org/10.1016/j.geomorph.2021.107990, 2021a.

Wang, J., Yang, S. T., Lou, H. Z., Liu, H. P., Wang, P. F., Li, C. J., and Zhang, F.: Impact of lake water level decline on river evolution in Ebinur Lake Basin (an ungauged terminal lake basin), Int J Appl Earth Obs, 104, 1-14, https://doi.org/10.1016/j.jag.2021.102546, 2021b.

Wang, L., Wang, X., Xu, X., and Cui, J.: What happened on the upstream of Minjiang River in Sichuan Province 20,000 years ago, Earth Science Frontiers, 14, 189-196,

https://www.earthsciencefrontiers.net.cn/CN/Y2007/V14/I6/189, 2007.
Wang, L., Yang, L., Wang, X., and Duan, L.: Discovery of huge ancient dammed lake on upstream of Minjiang River in Sichuan , China, Journal of Chengdu University of Technology, 32, 1-11, 2005a.
Wang, L., Yang, L., Wang, X., and Duan, L.: Discovery of huge ancient dammed lake on upstream of Minjiang River in Sichuan , China, Journal of Chengdu University of Technology (Science & Technology Edition), 32, 1-11, https://doi.org/CNKI:SUN:CDLG.0.2005-01-001, 2005b.
Wang, L., Wang, X., Xu, X., Cui, J., Shen, J., and Zhang, Z.: Significances of studying the diexi paleo dammed lake at the upstream of minjiang river, sichuan, China, Quaternary Sciences, 32, 998-1010, https://doi.org/10.3969/j.issn.1001-7410.2012.05.16, 2012.
Wang, L., Wang, X., Shen, J., Xu, X., Cui, J., Zhang, Z., and Zhou, Z.: The effect of evolution of Diexi ancient barrier lake in the upper Mingjiang River on the Chengdu Plain in Sichuan, China, Journal of Chengdu University of technology, 47, 1-15, https://doi.org/10.3969/j.issn.1671-9727.2020.01.01, 2020a.
Wang, L., Wang, X., Shen, J., Yin, G., Cui, J., Xu, X., Zhang, Z., Wan, T., and Wen, L.: Late Pleistocene environmental information on the Diexi paleo-dammed lake of the upper Minjiang River in the eastern margin of the Tibetan Plateau, China, Journal of Mountain Science, 17, 1172-1187, https://10.1007/s11629-019-5573-x, 2020b.
Wang, P., Zhang, B., Qiu, W., and Wang, J.: Soft-sediment deformation structures from the Diexi paleo-dammed lakes in the upper reaches of the Minjiang River, east Tibet, Journal of Asian Earth Sciences, 40, 865-872, https://doi.org/10.1016/j.jseaes.2010.04.006, 2011.
Wang, X.: The Environment Geological Information in the Sediments of Diexi Ancient Dammed Lake on the upstream of Mingjiang River in Sichuan Province, China, Chengdu University of Technology, Chengdu, 116 pp., 2009.
Wang, X., Li, C., Lv, L., and Dong, J.: Analysis of the late Quaternary activity along the Wenchuan-Maoxian fault-middle of the back-range fault at the Longmenshan fault zone, Seismology and Geology, 39, 572-586, https://doi.org/10.3969/j.issn.0253-4967.2017.03.010, 2017.
Wang, X., Li, Y., Yuan, Y., Zhou, Z., and Wang, L.: Palaeoclimate and palaeoseismic events discovered in Diexi barrier lake on the Minjiang River, China, Natural Hazards and Earth System Sciences, 14, 2069-2078, https://doi.org/10.5194/nhess-14-2069-2014, 2014.
Wang, Y., Cheng, H., Edwards, R. L., An, Z., Wu, J., Shen, C.-C., and Dorale, J. A.: A high-resolution absolute-dated late Pleistocene monsoon record from Hulu cave, China, Science, 294, 2345-2348, https://doi.org/10.1126/science.1064618, 2001.
Wang, Y., Cheng, H., Edwards, R. L., Kong, X., Shao, X., Chen, S., Wu, J., Jiang, X., Wang, X., and Wang, Z.: Millennial- and orbital-scale changes in the East Asian monsoon over the past 224,000 years, Nature, 451, 1090-1093, https://doi.org/10.1038/nature06692, 2008.
Westaway, R. and Bridgland, D.: Late Cenozoic uplift of southern Italy deduced from fluvial and marine sediments: Coupling between surface processes and lower-crustal

flow, Quaternary International, 175, 86-124, https://doi.org/10.1016/j.quaint.2006.11.015, 2007.
Wintle, A. G. and Murray, A. S.: A review of quartz optically stimulated luminescence characteristics and their relevance in single-aliquot regeneration dating protocols, Radiation Measurements, 41, 369-391, https://10.1016/j.radmeas.2005.11.001, 2006.
Wu, L., Zhao, D. J., Zhu, J., Peng, J., and Zhou, Y.: A Late Pleistocene river-damming landslide, Minjiang River, China, Landslides, 17, 433-444, https://doi.org/10.1007/s10346-019-01305-5, 2019.
Xu, H., Chen, J., Cui, Z., and Chen, R.: Sedimentary facies and depositional processes of the Diexi Ancient Dammed Lake, Upper Minjiang River, China, Sedimentary Geology, 398, https://10.1016/j.sedgeo.2019.105583, 2020.
Yang, F., Fan, X., Siva Subramanian, S., Dou, X., Xiong, J., Xia, B., Yu, Z., and Xu, Q.: Catastrophic debris flows triggered by the 20 August 2019 rainfall, a decade since the Wenchuan earthquake, China, Landslides, 18, 3197-3212, https://doi.org/10.1007/s10346-021-01713-6, 2021.
Yang, N., Zhang, Y., Meng, H., and Zhang, H.: Study of the Minjiang River terraces in the western Sichuan Plateau, Journal of Geomechanics, 9, 363-370, https://doi.org/10.3969/j.issn.1006-6616.2003.04.008, 2003.
Yang, W.: Research of Sedimentary Record in Terraces and Climate Vary in the Upper Reaches of Minjiang River, China, Chengdu University of Technology, Chengdu, 2005.
Yang, W., Zhu, L., Zhang, Y., and Kan, A.: Sedimentary evolution of a dammed paleolake in the Maoxian basin on the upper reach of Minjiang River, Sichuan, China, Marine Geology Frontiers, 27, 35-40, https://doi.org/CNKI:SUN:HYDT.0.2011-05-007, 2011.
Yang, W., Zhu, L., Zheng, H., Xiang, F., Kan, A., and Luo, L.: Evoluton of a dammed palaeolake in the Quaternary Diexi basin on the upper Minjiang River, Sichuan, China, Geological Bulletion of China, 27, 605-610, https://doi.org/10.3969/j.issn.1671-2552.2008.05.003, 2008.
Yang, Y., Li, B., Yin, Z., and Zhang, Q.: The Formation and Evolution of Landforms in the Xizang Plateau, ACTA GEORAPHICA SINICA, 76-87, https://doi.org/10.11821/xb198201009, 1982.
Yoshikawa, T., KaizukaYoko, S., and Ota, O.: Mode of crustal movement in the late Quaternary on the southeast coast of Shikoku, southwestern Japan, Geographical Review of Japan, 37, 627-648, https://doi.org/10.4157/grj.37.627, 1964.
Yu, Y., Wang, X., Yi, S., Miao, X., Vandenberghe, J., Li, Y., and Lu, H.: Late Quaternary aggradation and incision in the headwaters of the Yangtze River, eastern Tibetan Plateau, China, GSA Bulletin, 134, 371-388, https://doi.org/10.1130/b35983.1, 2021.
Yuan, G. and Zeng, Q.: Glacier-dammed lake in Southeastern Tibetan Plateau during the Last Glacial Maximum, Journal Geological Society of India, 79, 295-301, https://10.1007/s12594-012-0041-z, 2012.
Zhang, B., Wang, P., and Wang, J.: Discussion of the Origin of the Soft-Sediment Deformation Structures in Paleo-dammed Lake Sediments in the Upper Reaches of the Minjiang River, Journal of Seismological Research, 34, 67-74,

https://doi.org/10.3969/j.issn.1000-0666.2011.01.011, 2011.
Zhang, S.: Characteristics and Geological Significance of the Late Pleistocene Lacustrine Sediments in Diexi, Sichuan, China University of Geosciences, Beijing, 76 pp., 2019.
Zhang, X., David, H., Liu, W., and Tang, Q.: Terraces of Ancient Giant Jintang Landslide-dammed Lake in Jinsha River, Journal of Mountain Science, 31, 127, https://doi.org/10.16089/j.cnki.1008-2786.2013.01.019, 2013.
Zhang, Y., Zhu, L., Yang, W., Luo, H., Jiang, L., He, D., and Liu, J.: High Resolution Rapid Climate Change Records of Lacustrine Deposits of Diexi Basin in the Eastern Margin of Qinghai-Tibet Plateau, 40–30 ka BP, Earth Science Frontiers, 16, 91-98, https://doi.org/10.1016/s1872-5791(08)60106-2, 2009.
Zhao, X., Deng, Q., and Chen, S.: Tectonic geomorphology of the Minshan uplift in western Sichuan, southwestern China, Seismology and Geology, 16, 429-439, https://doi.org/CNKI:SUN:DZDZ.0.1994-04-017, 1994.
Zhong, N.: Earthquake and Provenance Analysis of the Lacustrine Sediments in the Upper Reaches of the Min River during the Late Pleistocene, Institute of Geology, China Earthquake Administration, Beijing, 193 pp., 2017.
Zhong, Y., Fan, X., Dai, L., Zou, C., Zhang, F., and Xu, Q.: Research on the Diexi Giant Paleo-Landslide along Minjiang River in Sichuan, China, Progress in Geophysics, 36, 1784-1796, https://doi.org/10.6038/pg2021EE0367, 2021.
Zhou, R., Pu, X., He, Y., Li, X., and Ge, T.: Recent activity of Minjiang fault zone, uplift of Minshan block and their relationship with seismicity of Sichuan, Seismology and Geology, 22, 285-294, https://doi.org/CNKI:SUN:DZDZ.0.2000-03-009, 2000.
Zhu, J.: A preliminary study on the upper reaches of Minjiang River Terrace, Chengdu University of Technology, Chengdu, 73 pp., 2014.
Zhu, S., Wu, Z., Zhao, X., and Keyan, X.: Glacial dammed lakes in the Tsangpo River during late Pleistocene, southeastern Tibet, Quaternary International, 298, 114-122, https://10.1016/j.quaint.2012.11.004, 2013.